DETERMINATION OF RESIDUAL STRESSES IN HSLA-100 STEEL WELDMENTS AS A FUNCTION OF WELDING PARAMETERS USING X-RAY DIFFRACTION

by

David R. Cunningham

Thesis submitted to the Faculty of the

Virginia Polytechnic Institute and State University

in partial fulfillment of the requirements for the degree of

MASTER OF SCIENCE

in

Materials Science and Engineering

APPROVED:

Prof. Robert W. Hendricks, Chairman

Prof. William T. Reynolds, Jr.

Prof. Norman E. Dowling

May, 1994

Blacksburg, Virginia

DETERMINATION OF RESIDUAL STRESSES IN HSLA-100 STEEL WELDMENTS AS A FUNCTION OF WELDING PARAMETERS USING X-RAY DIFFRACTION

by

David R. Cunningham

Thesis submitted to the Faculty of the
Virginia Polytechnic Institute and State University
in partial fulfillment of the requirements for the degree of
MASTER OF SCIENCE
in
Materials Science and Engineering

ABSTRACT

This project was initiated by the Carderock Division of the Naval Surface Warfare Center (CDNSWC) and the Office of Naval Research to study the effects of various processing parameters on the residual stress state of HSLA-100 bead-on-plate weldments. Three groups of samples were provided to Virginia Tech by CDNSWC. The first (GPX) was a sample of unwelded, as-received base material; the second group (RS-) consisted of an experimental matrix of differently processed bead-on-plate weldments which were all ground prior to welding in order to prepare the surface for welding; the third group (SR-) was a pair of weldments vacuum annealed at 1200°F for one and two hours, and then welded (without grinding) using welding parameters identical to weldments from the second group. X-ray diffraction was used to measure the surface residual stress state of all samples. It was found that the surface residual stress states of the GPX plate and the unwelded SR- group plates showed no statistically significant difference in magnitude, though the variation of the stress state over the surface of the plates seemed to decrease with increasing annealing time.

The severe, non-uniform grinding was determined to play a very large role in the residual stresses generated in the welds, sometimes changing both the magnitude and the shape of the stress patterns. Residual stresses in plates that were ground before welding were always more tensile than those that were not ground. Grinding also caused a large compressive-to-tensile stress gradient in the transverse direction. The grinding made it difficult to determine the effects of different welding parameters on the residual stress state.

Assuming that the stresses closest to the weld bead are exclusively residual stresses due to welding, preheat temperature reduced the tensile nature, or increased the compressive nature, of the residual stresses. This is due to the preheat reducing the effect of shrinkage stresses induced after the austenite transformation upon cooling of the weldment. Because of the effects of grinding and the small sample sizes, no definitive conclusions could be drawn about the effects of heat input and plate thickness. It was shown that grinding was the dominant parameter on the residual stress state in these HSLA-100 bead-on-plate weldments. Because the angle and force of grinding are purely at the discretion of the operator, it is very difficult to determine the effects of different welding parameters on the residual stresses generated in bead-on-plate weldments ground prior to welding.

ACKNOWLEDGMENTS

Financial support for this project originated with Mr. Joe Blackburn and the Carderock Division of the Naval Surface Warfare Center and was provided by Dr. George Yoder under the Office of Naval Research Project Award No. N0001489J1351P00005. Mr. Blackburn and the Carderock Division of the Naval Surface Warfare Center provided all of the necessary materials and the processing of those materials. Mr. Blackburn also provided various sorts of assistance in the form of information concerning the material and it's processing. Additional financial support was provided by Dr. Ronald S. Gordon and the Materials Science and Engineering Department at Virginia Polytechnic Institute and State University. Other economic assistance was provided by Mr. Mike Brauss of Proto Manufacturing.

Of course, none of this work would not have been possible without the generous aid of my three committee members, most notably Professor Robert W. Hendricks. He did a superb job of balancing the line between providing assistance and encouraging me to tap into my own personal resources. He both understands and supports having a wide-range of interests, and never balks at the seeking of an answer. What I will remember most is his kindness and thoughtfulness, for of both he has an abundance. Professor William T. Reynolds has been a part of my education the longest, for he also advised me in my undergraduate studies. I will always remember his knowledge of metallurgy and his willingness to inconvenience himself for the convince of students. I have personally witnessed Dr. Reynolds miss many a meal in order to satisfy the queries of an student seeking unscheduled assistance. Professor Norman E. Dowling was a valuable source of information, and was very interested that the knowledge he communicated was being received clearly. I would also like to thank Professor Robert V. Foutz of the Statistics Department at Virginia Tech for his repeated help in analyzing the mass quantities of data generated by this project.

Many colleagues deserve recognition for the assistance they provided, either formally or otherwise. Heidi Allison joined the project upon completion of her Bachelor's of Science degree, and her aid was invaluable to the conclusion of this phase of the work. Benoit Girardin was very kind with the scheduling of computer time in order for me to finish this thesis in an opportune

fashion. Scott Courtney showed unending patience when answering questions about a broad range of topics, from technical writing to computer systems. Bill Halley was always quick with a very informative answer to any question, whether about metallurgy or general engineering. Ken Venzant provided the initial instruction on the diffraction equipment upon which so much time was spent. Marc Tricard helped me off to a good start towards understanding life as a graduate student. Others whose aid deserves mentioning are Eric Wuchina, Bill Russ, Mike Stawovy, Mike Farrell, Greg Moeller, and the outstanding office staff of the Materials Science and Engineering department.

Naturally, none of this would have been possible without the help of my family, both nuclear and extended. My mother, Sandra L. Cunningham, deserves the most credit for never failing to be there when needed, while at the same time never passing judgment (at least not audibly :-). There is a myriad of grandparents, aunts, uncles, and cousins who all provided aid in many forms, most unknowingly, though some knowingly. I thank them each and think of them often. I firmly believe that a loving family is the foremost asset a person can have.

TABLE OF CONTENTS

LIST OF FIGURES

LIST OF TABLES

1. INTRODUCTION

The Carderock Division of the Naval Surface Warfare Center and the Office of Naval research are conducting and providing for research leading to the certification of a new HSLA-100 steel alloy. This alloy is meant to replace the HY-100 alloy currently being used for surface combatant and submarine non-pressure hull structural ship applications. The objective of the replacement program is to reduce fabrication costs and meet or exceed the strength requirements of the original alloy. The results of a similar program, which successfully replaced a HY-80 steel with a HSLA-80 alloy, led to the development of the present comparable program.[1]

Before the replacement can take place, a full certification of the new HSLA-100 steel alloy must occur. Part of this certification process is understanding the role of residual stresses in HSLA-100 steels, because these stresses may cause distortion and cracking in welded parts. The stress relieving of large structures is not feasible, so it is the objective of the Carderock Division of Naval Research (CDNSWC) to be able to determine, predict, and eventually model the formation and distribution of weld residual stresses in HSLA-100 steels.[2]

In order to achieve these goals, the relationship between welding processing parameters and residual stress must be explored. The study of this relationship is a major step towards gaining the ability to predict and model residual stresses in welded parts. Due to the numerous welding parameters, a large number of samples is required to initiate such a study. In addition, the stress determination method must be fast enough to gain the information desired in a reasonable amount of time. It is also desirable that the method be non-destructive in order to preserve the integrity of the structures being examined. X-ray diffraction is a well known, non-destructive method of residual stress determination which is more reliable than some non-destructive methods (such as ultrasonic techniques or Barkhausen Noise Analysis), and faster than others (neutron diffraction).

The objective of this thesis is to begin the development the science and technology that permits the prediction of the distribution of residual stresses in gas-metal arc-welded (GMAW)

HSLA-100 structural steels as a function of welding process and procedural variables such as material thickness, welding current, potential, travel speed, and preheat temperature. This is accomplished using x-ray diffraction to determine the surface residual stress state in an experimental matrix of differently processed HSLA-100 steel welds. In addition, scientists at the National Institute for Standards and Technology are using neutron diffraction to study the internal stresses generated in weldments. The resulting data from both projects will be used by scientists at Oak Ridge National Laboratory to aid in the development of mathematical models for welding residual stresses.

2. BACKGROUND

2.1 HSLA Steels

High-Strength, Low-Alloy (HSLA) steels are exactly that: high strength steels with low levels of those alloying elements usually associated with strength in steels. They were originally developed as a method of cost savings in the manufacture of transportation equipment, and this remains where the largest amount of HSLA steels are consumed.[3] When compared with other structural steels used for similar purposes, the greater strength of HSLA steels allows for increased weight savings due to the lesser amount of material needed to meet the same structural requirements. The higher cost/weight ratio of HSLA steels is compensated for by the better cost/strength ratio. HSLA steels are also desirable due to their higher durability, abrasion resistance, and in some instances, atmospheric corrosion resistance. High-strength, low-alloy steels are available under a variety of names, such as microalloyed steels, weathering steels, or controlled-rolled steels. To make identification even more difficult, a given composition HSLA steel will have several proprietary names, each depending on the particular manufacturer.

One of the more intriguing aspects of HSLA steels is the high yield strength attained without the higher carbon content normally associated with high strength steels. The lower carbon content decreases hardenability which increases weldability, another advantage of this group of steels. The higher strength of these steels is attained through special processing and the addition of small amounts of precipitate-forming elements such as niobium, titanium, vanadium, and copper.[4,5] Other alloying elements include manganese which is added to avoid the formation of iron sulfide and for better low temperature properties, phosphorus for increased strength (but decreased ductility) and increased atmospheric corrosion resistance (especially when copper is also present). Silicon acts as a deoxidizer while also increasing hardenability; chromium enhances corrosion resistance and strengthens HSLA steels containing copper and vanadium. Nickel increases strength

somewhat while enhancing corrosion resistance, especially to seawater corrosion when copper and/or phosphorous are/is also present. Molybdenum also acts as a strengthener in HSLA steels. Copper enhances corrosion resistance and acts as a solid-solution strengthener; newer HSLA alloys contain copper acting as a precipitation strengthener.[6]

Most HSLA steels are hot rolled. This processing increases the strength of the alloy by reducing the size of the austenite grains present in the preheated alloy, thus creating a fine subgrain structure upon cooling. Hot rolling also results in strain-induced precipitates which serve to pin the austenite grain boundaries, inhibiting grain growth. Ferrite grains nucleate on austenite grain boundaries, so the finer the austenite grain structure, the more nucleation sites there are for ferrite formation. Because strength is inversely proportional to the square root of the grain size, the fine ferrite microstructure leads to high strength in HSLA steels. The typical grain size of a HSLA steel is approximately one tenth the size of a plain alloy steel (this will be discussed further in Section 3.1).[7] Additional strengthening occurs when any remaining alloying elements precipitate into the ferrite as the steel cools.[8]

While HSLA steels have a higher cost/weight ratio, their cost/strength ratio (or strength/weight ratio) is more desirable than most of the other steels used for the same applications. Their ease of welding is also a major benefit; this makes them appropriate for many applications in which plain carbon steels are used. Some examples of such uses include: bridges, buildings, heavy construction and mining equipment, and defense-related purposes. Because of their high-strength and their low content of expensive alloying elements, HSLA steels are considered to be "one of the most important, and metallurgically interesting, modern engineering materials."[9]

2.2 Residual Stress due to Welding

Residual stresses are stresses that remain in a material after the removal of all externally applied load. Sometimes referred to as internal or inherent stresses, residual stresses are present in virtually all manufactured products. They result when a part is plastically deformed in a non-uniform manner, and the lattice must distort elastically in order to remain coherent. Residual stresses are especially sensitive to the non-uniform heating and cooling which takes place in all heat treated parts of appreciable thickness.[10] If the material is multiphase, both residual macrostresses and residual microstresses will exist. Residual macrostresses vary over a distance that is large as

compared to the microstructure and are equal in all phases of the material. Macrostresses result from unequal deformation of adjacent regions of material. Residual microstresses vary on the scale of the microstructure and result from differing thermal or elastic properties of the phases. Microstresses must balance to zero between the different phases of the material.[11] The sum of all of the residual stresses in a part must also balance to zero within that part.

Residual stresses are important because they combine with any applied stress to have either beneficial or deleterious effects. Surface tensile residual stresses combine with any tensile applied stresses and enhance the likelihood of fatigue cracking, stress corrosion cracking, and/or fracture. Internal tensile residual stresses may cause cracking when in the presence of internal defects which act as stress raisers.[12] Conversely, surface compressive residual stresses are beneficial because they reduce the effect tensile stresses have on the fracture mechanisms. Compressive residual stresses sum with any applied stress just as the tensile stresses do, but compressive residual stresses reduce the effect of any applied tensile load. Unfortunately, either type of residual stress may cause distortion of the workpiece leading to mismatch between mating parts.

The welding of a material consists of strong localized heating of an area with respect to the surrounding metal and always results in residual stress. The main stress generators associated with the heating and cooling imparted by the welding process are shrinkage and phase transformations. The inhomogeneity of thermal processes results in shrinkage in the welded metal and yielding of the surrounding higher temperature material.[13] A phase transformation and accompanying volume change will be restrained by the surrounding material resulting in residual stresses within the transformed and surrounding metal. Because of their proximity to a moving heat source, residual stresses in the vicinity of a weld are very complicated in nature and exhibit large gradients.[14,15] This may lead to adverse effects because residual stresses can play a large part in crack propagation.

The concepts of longitudinal (σ_l) and transverse (σ_t) residual stress will be used frequently throughout this text. In order to clarify what is meant by these terms, a diagram of the measurement directions on a schematic bead-on-plate weldment is shown in Figure 1. In Figure 1 and all other weldment diagrams, the bottom of the weld bead is its starting point and the top is the end point. All residual stress data was taken along a measurement line perpendicular to the length of the weld bead, at it's approximate midpoint.

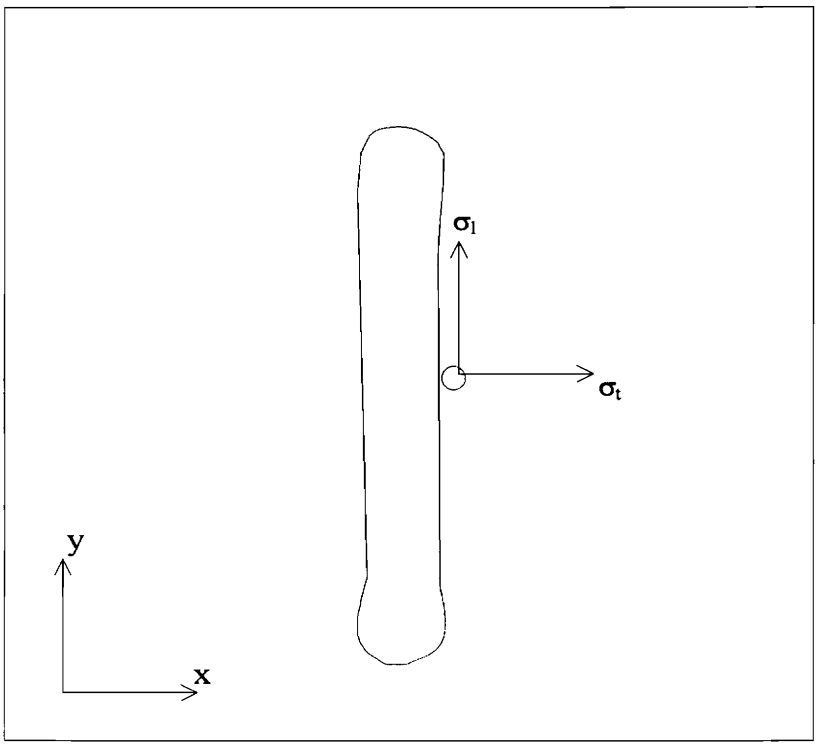

Figure 1. Schematic diagram of a standard bead-on-plate weldment, showing translation directions and the directions of transverse (σ_t) and longitudinal (σ_l) residual stress measurements.

If shrinkage was the only stress generating process, surface residual stresses on a line perpendicular to the weld bead would appear as shown in Figure 2.[16] Longitudinal residual stresses would be tensile in the weld bead and in the surrounding region (the material that cooled last), balanced by compressive residual stresses further away from the weld center line. Transverse residual stresses would be tensile across the plate, the magnitude of which depends on the welding process parameters.

However, shrinkage is not the only stress generating process; phase transformations also induce residual stress. If residual stresses due to the volume expansion associated with the austenite to bainite and/or martensite phase transformation (as is the case in HSLA-100) were the only stress generating process, the stresses would appear as shown in Figure 3.[17] Transverse residual stresses are compressive in both the transforming region and the surrounding material. Longitudinal residual stresses are compressive within transformed grains of material, and tensile outside of this transformed zone.

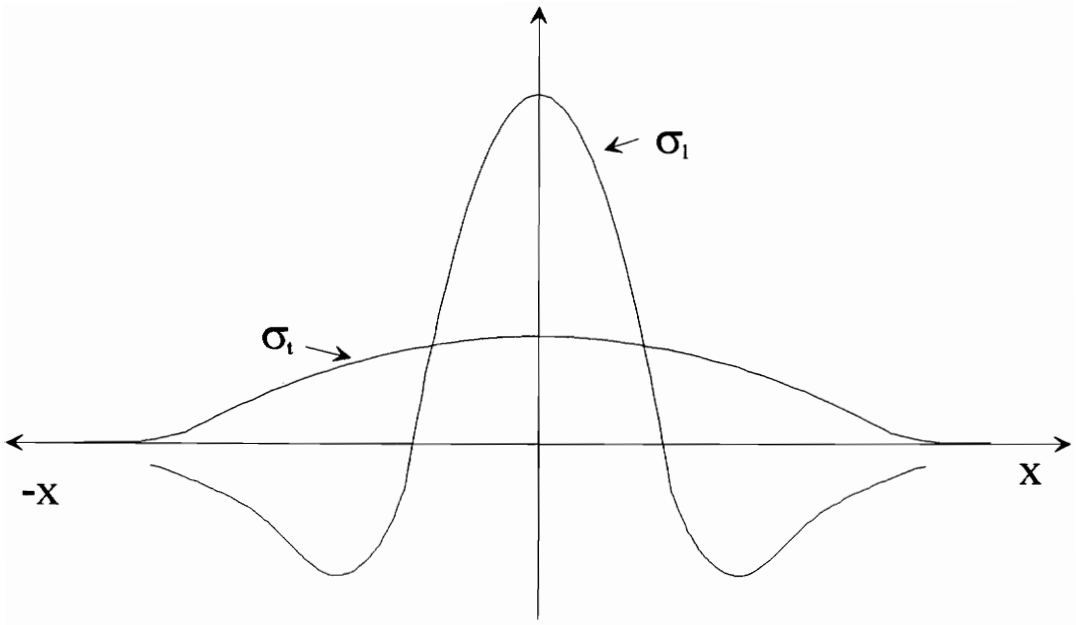

Figure 2. Welding residual stresses generated exclusively by the shrinkage process.

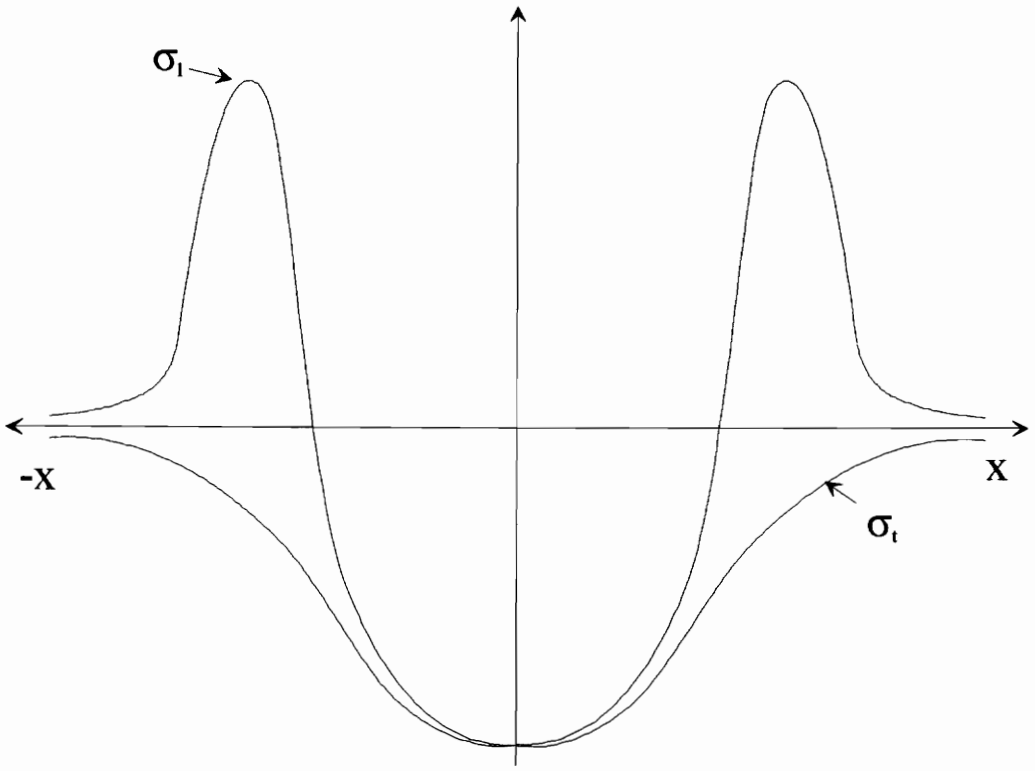

Figure 3. Welding residual stresses generated exclusively by phase transformations.

It is usually a combination of these two stress generating processes that result in the final residual stress state. Shrinkage occurs continuously as the heated material cools from its peak welding temperatures, causing tensile residual stresses. When austenite (γ) begins its transformation, compressive stresses are generated in the transforming region for the duration of the transformation. The final residual stress state depends on the temperature at which the austenite transformation takes place,[18] and thus depends on the cooling rate, which is in turn affected by the processing parameters such as heat input and preheat temperature. For a slow cooling rate, the γ-transformation will be complete at a high temperature, allowing for shrinkage stresses to increase the tensile component of the stress upon completion of the transformation. A fast cooling rate results in a low temperature γ-transformation, leaving little time for shrinkage after the transformation is complete. This results in a less tensile or more compressive stress state, depending on the magnitude of the shrinkage and/or transformation stresses.

Because of the sensitivity of the γ-transformation to different material and welding parameters, many factors affect the residual stresses generated in a welded material. Welding process parameters, such as preheat temperature, current, potential, and travel speed, as well as material parameters, such as weld joint geometry, thickness, thermal conductivity, and coefficient of thermal expansion all play a part in the residual stress state of a finished weldment. The welding current, potential, and travel speed are directly related to the heat input of the weld, as is described in the following equation:

$$h = 60 * \frac{VI}{\nu} \qquad (1)$$

where h is the heat input (J/in), V is the potential (V), I is the current (A), and ν is the travel speed (in/min). Controlling heat input is important in order to control the cooling rate of the weldment. If the part cools too quickly, brittle martensite may form and result in cracking. If the part cools too slowly, unwanted tempering of the heat-affected structure may take.[19] Heat input is directly related to the location of the maximum longitudinal residual stress.[20]

Preheating a structure before welding allows the entire thickness to reach a uniform temperature. Upon cooling after welding, stresses induced by shrinkage stop increasing when the preheat temperature is reached. Thus, adjustment of the preheat temperature can lower the peak tensile residual stress generated within a weldment.[21] Preheating also maintains the temperature of

the heat affected zone (HAZ) allowing hydrogen, which might eventually result in hydrogen cracking, to diffuse out of the part.[22]

Different stresses are known to cause cracking in different areas of a weldment. Transverse residual stresses, the more important component when fracture in the base material is the primary consideration, are also influenced by the length of the weld bead with respect to the plate and by the travel speed.[23] Longitudinal residual stresses are usually tensile in the vicinity of the weld bead and responsible for cracking within the weld bead itself.[24]

In typical welds, the interpretation of residual stress is difficult because of the large number of variables within the welding process. Dahl states that, "Due to the large number of welding parameters, groove geometries, plate dimensions, base and filler materials, and their effect on the formation of residual stresses, the results of residual stress measurements can be varying. This makes it difficult to categorize the types of weldments in relation to residual stress distribution."[25] Wohlfahrt includes, "It is therefore easy to understand how individual authors can report totally different welding stress distributions."[26]

2.3 X-ray Determination of Residual Stress

The determination of residual stresses may be accomplished either destructively or non-destructively. Destructive methods necessitate the removal of an amount of material, measuring the relaxation which takes place in the remaining material, and computing the stress from the strain redistribution which takes place (i.e., sectioning or hole drilling).[27] Methods such as these only measure macrostresses and reduce the structural integrity of the part being studied. Non-destructive methods of residual stress determination are preferable because they do not end the serviceability of the part.

X-ray diffraction (XRD) is "the most widely used, and the furthest advanced, method for evaluating residual stresses nondestructively."[28] In addition, the "x-ray method of measuring stresses is nondestructive and, after half a century of use, it is the standard to which other techniques must be compared."[29] It is easily the most accurate of the non-destructive methods; however, it does have certain limitations. For example, only the surface stress state is measured because the depth of penetration of the x-rays is typically only a few microns. In addition, the grains of the material must be randomly oriented and small enough that the x-ray beam will sample a

large number of grains with a random distribution of planar normals throughout space. This could be a problem when using x-rays to determine residual stress in weldments due to the grain growth which occurs in and near the HAZ.

The principle behind x-ray determination of residual stress (XRDRS) uses the planar lattice spacing of the material as an internal strain gauge. X-rays measure the lattice spacing, and the strain is computed from the distortion of the lattice. The most common (and recommended) method of XRDRS in use today is the $\sin^2\Psi$ technique.[30] Diffraction occurs when incident radiation of the proper wavelength, λ, strikes grains of material with the proper d-spacing, d_{hkl}, and orientation, θ. This is described by Bragg's law,

$$\lambda=2d_{hkl}\sin\theta, \qquad (2)$$

and is pictured in Figure 4. When λ and θ are known, Bragg's law may be used to determine d_{hkl}. This is the procedure used in XRDRS. Monochromatic x-rays of a known wavelength are used to irradiate a sample, and the resulting diffraction peak identifies the interplanar spacing of the grains of material being examined. If the unstressed lattice spacing, d_o, is known, the resulting strain, ε, in the diffracting grains may be determined from $\varepsilon = \frac{\Delta d}{d_o}$, where Δd is the change in the lattice spacing caused by the stress field. Hooke's law may then be used to compute the stress from the experimentally determined strain.

If a material is polycrystalline with randomly orientated grains, the normals of these differently oriented planes are uniformly distributed throughout space (N, Figure 4). Only those sets of planes with their normal bisecting the angle between the incident and diffracted x-rays diffract. By changing the orientation of the diffractometer with respect to the sample, different grains will diffract. Differently oriented planes will react in a different way to the same stress field. The d-spacing of a set of planes parallel with the surface of a sample undergoing tensile stress will decrease due to the Poisson's effect. The d-spacings of planes perpendicular to the surface of the sample will increase in the presence of a tensile stress field. The opposite will occur in compression, and a degree of one of the other will occur when the lattice planes are at an angle with the surface.

Figure 5 demonstrates the coordinate systems used for XRDRS. The S axes define the

sample coordinate system, with S_1 and S_2 in the plane of the material surface and S_3 normal to the sample surface. The L, or "laboratory" system, begins with the same orientation, but is then rotated by an angle ψ about L_2, and then rotated by an angle ϕ about L_3. In some instances, it is necessary to tilt the L_1 - L_3 plane with respect to the S_3 vector by an angle, χ. In this case, the interpretation of diffraction data becomes very complex, and can be found (including error analysis) in a paper by Jo and Hendricks.[31]

The relationship between the changes in d-spacings and an applied triaxial stress field can be determined using Cartesian coordinate system transformations, Hooke's law, and the strain-deformation relationship. For isotropic materials in which χ=0, the result is[32]

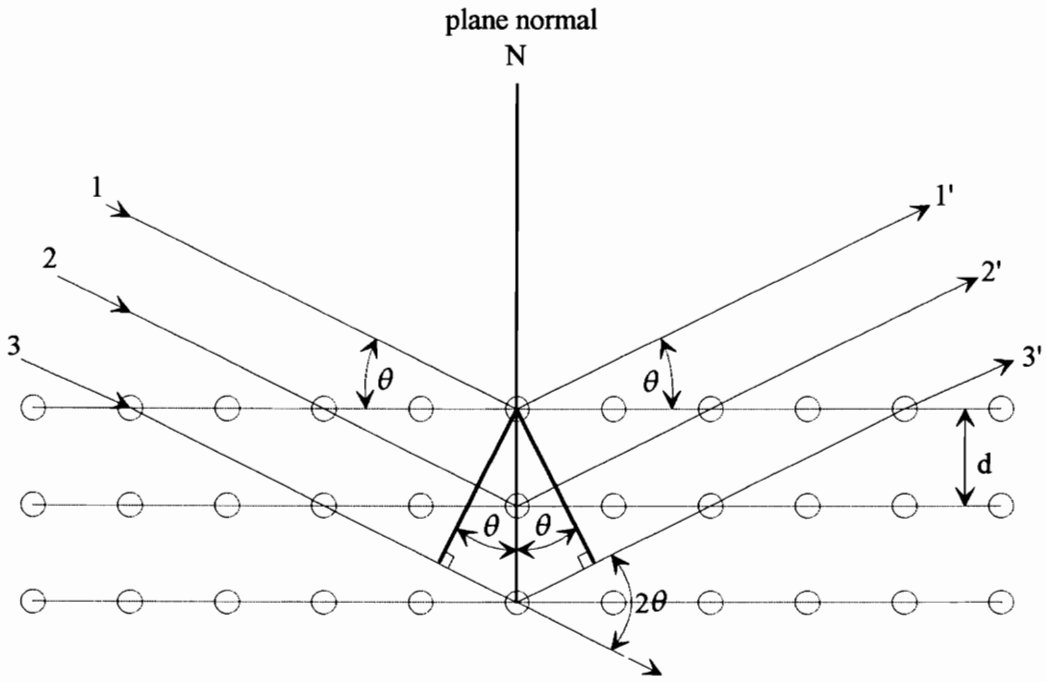

Figure 4. Diagram of Bragg's law: diffraction of incident radiation by atomic lattice planes, where θ is the angle between the diffracting planes and the incident radiation of wavelength λ, and d_{hkl} is the distance between the diffracting planes.

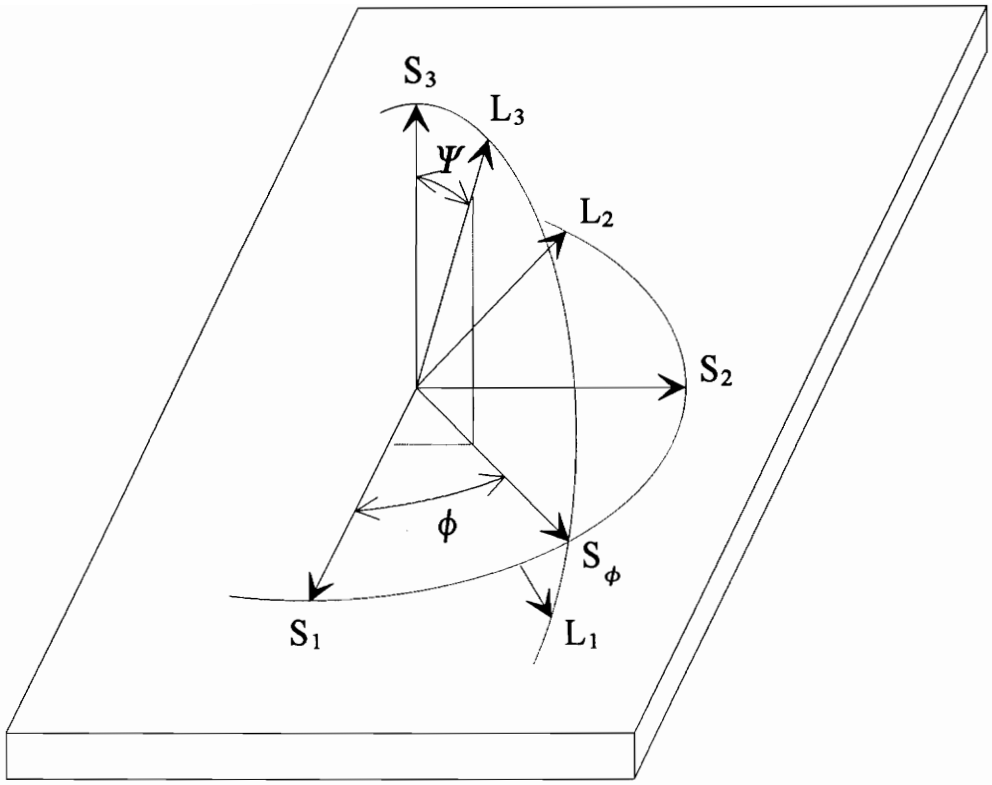

Figure 5. XRDRS coordinate systems where S_i is the sample coordinate system, L_j is the laboratory coordinate system, ψ is the angle between the sample normal and the normal of the diffracting planes, and ϕ is orientation of the laboratory system with respect to the sample system.

$$\frac{d_{\phi,\psi} - d_0}{d_0} = \varepsilon_{\phi,\psi} = \frac{1}{2}S_2(\sigma_{11}\cos^2\phi + \sigma_{12}\sin 2\phi + \sigma_{22}\sin^2\phi - \sigma_{33})\sin^2\Psi$$

$$+ \frac{1}{2}S_2\sigma_{33} + S_1(\sigma_{11} + \sigma_{22} + \sigma_{33}) \qquad (3)$$

$$+ \frac{1}{2}S_2(\sigma_{13}\cos\phi + \sigma_{23}\sin\phi)\sin 2\psi$$

where S_1 and S_2, the x-ray elastic constants, are specific to both the radiation wavelength and the (hkl) planes being examined; $d_{\phi,\psi}$ is the d-spacing of the planes with a normal having the orientation (ϕ,ψ) with respect to the S coordinate system (see Figure 5); and σ_{ij} are the components of the triaxial stress tensor.

The x-ray elastic constants are given by

$$S_1(hkl) = -\frac{\nu}{E_{hkl}} \tag{4}$$

and

$$\frac{1}{2}S_2(hkl) = \frac{1+\nu}{E_{hkl}} \tag{5}$$

where E_{hkl} is the Young's modulus of the hkl planes and ν is Poisson's ratio. The x-ray elastic constants differ from bulk elastic constants (Young's modulus) because the value of Young's modulus is different for different sets of hkl planes.

At ψ=0, (3) reduces to

$$\frac{d_{\phi,0} - d_0}{d_0} = \frac{1}{2}S_2\sigma_{33} + S_1(\sigma_{11} + \sigma_{22} + \sigma_{33}). \tag{6}$$

Subtracting (6) from (3) gives

$$\frac{d_{\phi,\Psi} - d_{\phi,0}}{d_0} = \frac{1}{2}S_2\sigma_\phi \sin^2\Psi + \frac{1}{2}S_2(\sigma_{13}\cos\phi + \sigma_{23}\sin\phi)\sin 2\Psi \tag{7}$$

where

$$\sigma_\phi = \sigma_{11}\cos^2\phi + \sigma_{12}\sin 2\phi + \sigma_{22}\sin^2\phi - \sigma_{33} \tag{8}$$

is the stress in the ϕ direction (S_ϕ in Figure 5). If the unstressed lattice spacing is known, it is possible to calculate the entire stress tensor. Unfortunately, d_o is generally not known and is difficult to determine. The $\sin^2\Psi$ method allows for the calculation of the residual stress in the S_ϕ direction even when the unstressed lattice spacing is unknown, by substituting the d-spacing at ψ=0° as measured by XRD for d_o. For most materials, elastic strain will not exceed 0.1%. Equation (7) shows that the unstressed lattice spacing is only a multiplier of the stress; hence, an error of <0.1% in d_0 results in an equal magnitude error in σ_ϕ, which may be disregarded when compared to the possible errors caused by misalignment, statistical analysis, or instrumentation.[33]

If the stresses are assumed to be biaxial, as is the case in most XRDRS because of the relatively shallow depth of penetration of the x-rays, (7) and (8) reduce to

$$\frac{d_{\phi,\Psi} - d_{\phi,0}}{d_0} = \frac{1}{2}S_2\sigma_\phi \sin^2\Psi \tag{9}$$

and

$$\sigma_\phi = \sigma_{11}\cos^2\phi + \sigma_{12}\sin 2\phi + \sigma_{22}\sin^2\phi \qquad (10)$$

respectively. Equation (9) shows that a plot of the d-spacings versus $\sin^2\Psi$ will be a straight line with a slope σ_ϕ, as can be seen in Figure 6a and Figure 10 (p. 22). However, if shear stresses exist in the plane of rotation of the diffractometer, the $\sin 2\Psi$ term of (7) causes a "split" in the d vs. $\sin^2\Psi$ plot for non-zero values of ψ, as can be seen in Figure 6b. This is often seen in practice and is evidence of shear stress existing in the material under investigation.

Other disparities from the above assumptions will result in other artifacts in the d vs. $\sin^2\Psi$ plot; for example, a strong stress gradient perpendicular to the surface of the material may be detected by a gradual curve in the d vs. $\sin^2\Psi$ plot caused by a decrease in the depth of penetration of the x-rays with increasing magnitudes of ψ (Figure 6c).

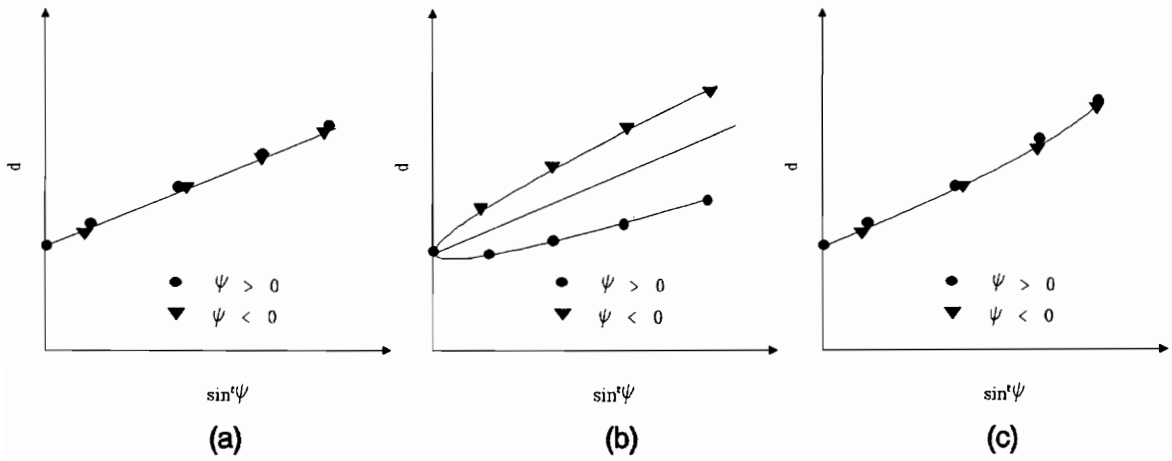

Figure 6. Typical d vs. $\sin^2\Psi$ plots: (a) "good" straight line plot of data with slope = σ_ϕ, (b) plot showing the effect of shear, and (c) a plot with curve indicating a stress gradient perpendicular to the surface of the material.

3. MATERIALS AND METHODS

3.1 HSLA-100 Steel

All weldments and weld base plate material were prepared and provided by the Carderock Division of the Naval Surface Warfare Center. The steel used for this research was produced by Phoenix Steel Corporation, Claymont Works. Additional plates were produced from Phoenix ingots by Lukens Steel Company, Coatesville, PA. The plates of HSLA-100 steel were solution heat treated at 1650°F for one hour and quenched using high pressure water jets. The quench water did not exceed 85°F in order to guarantee the proper cooling rate. After quenching, the production plates were age hardened at proper temperatures and times in order to achieve tensile strength of between 100-120 ksi. The proper heat treatments were determined by tensile testing specimens which underwent different aging conditions, and using comparable aging treatments on the production plate.[34]

The chemical composition of the HSLA-100 steel alloy used throughout this investigation is shown in Table 1. The higher copper content than most HSLA steels induces additional strengthening in the form of precipitation strengthening; while the high nickel content lowers the impact toughness transition temperature, it also lowers the upper shelf impact toughness. Hardenability is increased due to additions of manganese, nickel, and molybdenum. Most steel welds are susceptible to cracking in the HAZ where brittle martensite has formed. HSLA steels have the opposite problem: they have a reputation for softening in the HAZ due to grain growth and the dissolution of precipitation strengthening elements. The addition of the hardenability increasing elements counteracts the softening of the metal in this region of the weldment, thus creating a steel with excellent weldability.[35]

Some bulk mechanical properties of the HSLA-100 steel alloy used in this experiment are reported by Czyryca, et. al. to be: Young's modulus 29 X 10^6 psi; Poisson's ratio 0.3; and yield

Table 1. Nominal chemical composition of HSLA-100 steel alloy used in this research.

C	Mn	Si	Ni	Cr	Mo	Cu	Cb	Al	S	P	N
0.04	0.90	0.25	3.50	0.60	0.60	1.60	0.025	0.03	0.003	0.006	0.010

strength minimum 100 ksi (hence the name, HSLA-100). Corrosion properties are especially important because of the environment in which this alloy will be used. Of particular importance is the susceptibility to stress corrosion cracking (SCC), "since complex, welded heavy-section structures result in high residual tensile stress states in the vicinity of weldments." Extensive testing revealed that corrosion rates for this alloy (including SCC rates) were roughly equivalent to the corrosion rates of most structural steels. In addition, no preferential corrosion took place on any one area of the weldments (base metal, HAZ, and/or weld bead).[36]

The microstructure of the HSLA-100 steel alloy was determined by scanning electron microscopy to be a fine-grained mixture of low-carbon martensite and lower bainite in thin plates, and primarily bainite in thick plates [CDNSWC].[37] At Virginia Tech, quarter inch bar was cut from the end of a sample of as-received base plate perpendicular to the rolling direction. Three samples were cut from this piece in order to examine each of the three faces of the base plate metallographically. The original location of these specimens is shown in Figure 7. The three samples were mounted, ground, and polished using standard metallographic procedures, and etched using 2% nital. The micrographs of these specimens are shown in Figure 8.

The average grain size of 3/4-inch plate was reported to be 8.5 μm.[38] This grain size should be conducive to good x-ray diffraction. A small grain size allows for the diffraction data to average over a large number of grains, which is the desired situation. The depth of penetration of x-rays used to determine the residual stress state in steel is small (approximately 5.5 μm).[39] Comparison of the grain size and the effective depth of penetration of the x-rays shows that XRD is determining the residual stress state in a layer of material less than the size of a single grain. Grain growth is expected in the vicinity of the weld bead; however, the diffraction data is expected to reveal any anomalies that might be associated with the grain structure. No significant texture was observed or reported in other work.[40]

All welding was performed with MIL-120S-1 welding consumables. The nominal chemical composition of this welding wire is shown in Table 2.[41]

Table 2. Nominal chemical composition of as-deposited weld metal.

C	Mn	Si	Ni	Cr	Mo	Cu	Zr	Al	S	P	V, Ti
0.07	1.54	0.36	2.28	0.29	0.47	0.01	0.01	0.02	0.005	0.007	<0.01

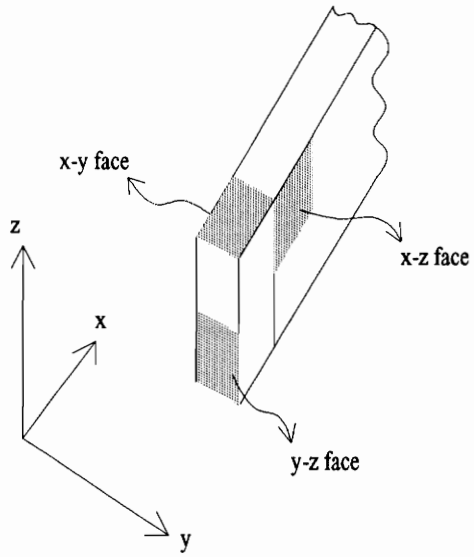

Figure 7. Original location of metallography specimens cut from the GPX as-received base material.

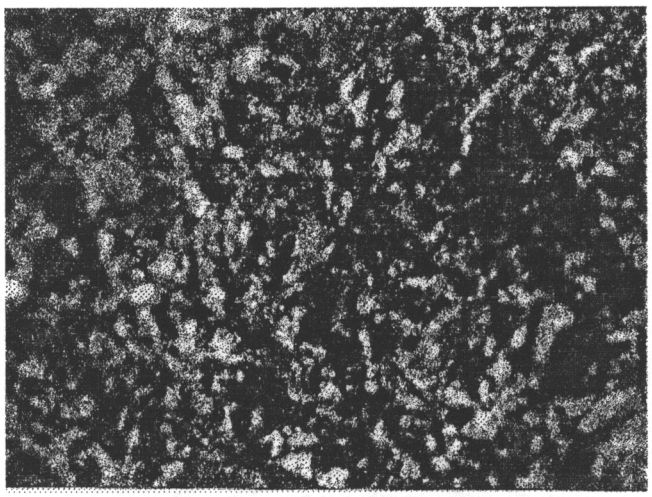

(a) x-y face.

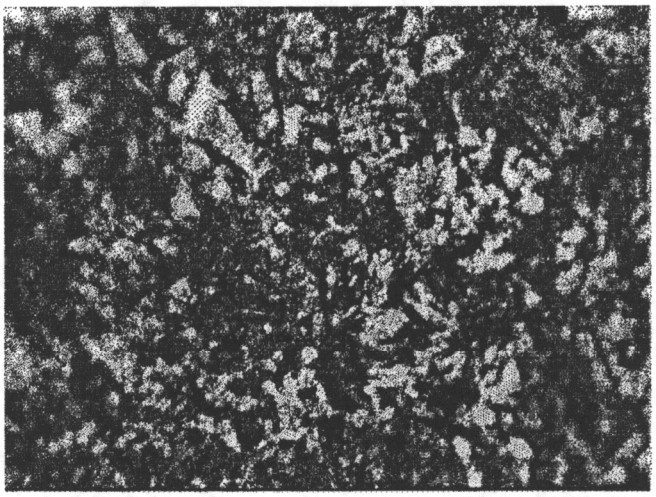

(b) x-z face.

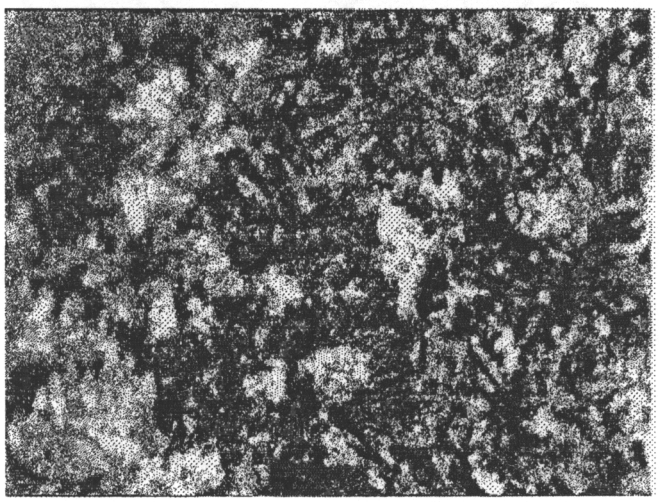

(c) y-z face.

Figure 8. Optical micrographs of the GPX as-received HSLA-100 base plate.

3.2 X-ray Diffraction Parameters

The residual stress data were gathered using a Technology for Energy Corporation (TEC) Model 1610 Portable Apparatus for Residual Stress (PARS).[42] Vanadium-filtered chromium K_α radiation of wavelength 2.290920 Å was diffracted from the (211) planes of iron at 156° 2θ. The diffraction intensities associated with high 2θ angles are not as strong as the diffraction intensities of lower diffraction angles, but shifts in 2θ are easier to detect at high values of 2θ.

Data were collected at seven ψ angles, between -45° and 45°. Measurement times were optimized to produce the lowest counting statistics errors in the most reasonable amount of time. Section 4 discusses counting statistics errors in greater detail. Transverse measurements were made using a 2 x 5 mm slit collimator, with the length of the slit parallel to weld bead in order to reduce the effect of any possible stress gradient in the transverse direction. In the longitudinal direction and on unwelded base plates, a two millimeter diameter round collimator was employed because no significant stress gradient was expected. Different collimators require different measurement times to attain the same statistical accuracy per measurement, as will also be discussed further in Section 4.

The x-ray elastic constant, $\frac{1+\nu}{E_{hkl}}$, used to compute stress from strain is 3.50×10^{-8} psi. This is the published value for the (211) planes of an HSLA 328 steel.[43] Although not the x-ray elastic constant for our particular material, using this value was not viewed to be a problem because the differences between the x-ray elastic constants of two types of HSLA steels is not expected to be great. In addition, the x-ray elastic constant is only a multiplier of the slope (just as is the unstressed lattice spacing), and minor corrections in the x-ray elastic constant will result in small changes in the reported residual stress values. Also, for the purposes of this thesis, relative stress values that are more important than the actual magnitudes of those stresses. A slight discrepancy of the x-ray elastic constant will not interfere with the comparison of residual stresses generated by different welding parameters.

A typical diffraction pattern is shown in Figure 9, with the x-axis representing the 2θ angle and the y axis representing the intensity of the diffracted x-rays. The diffraction peaks obtained from annealed steel samples are very narrow due to uniformity in the lattice spacings among the

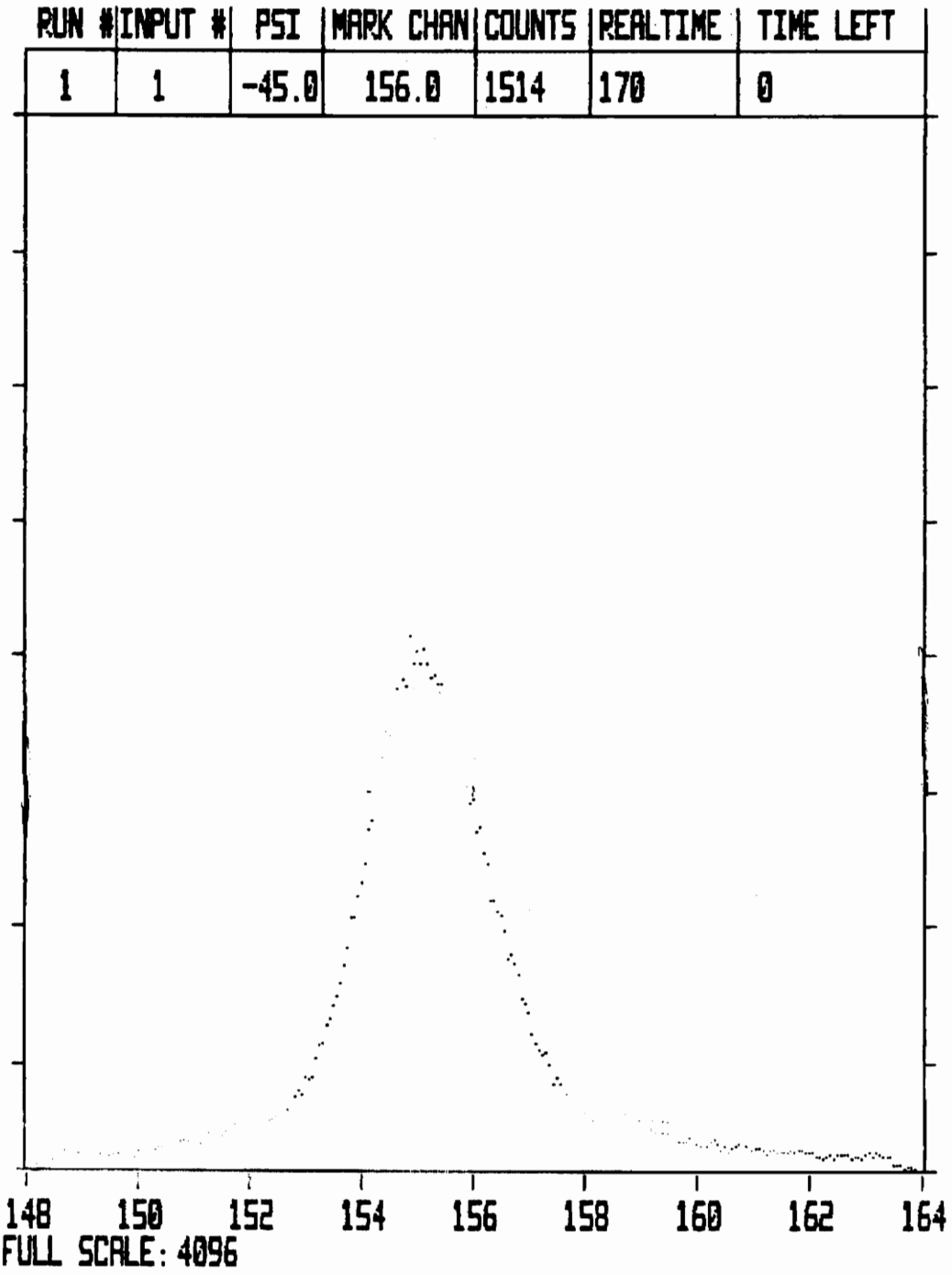

Figure 9. Typical x-ray diffraction pattern with the x-axis representing channel numbers in the position sensitive proportional detector which are directly calibrated to 2θ, and the y-axis representing the number of x-ray photons detected per channel.

grains examined. Cold-working steel results in peak-broadening due to large variations in d-spacings caused by localized stress fields within the material. A typical d vs. $\sin^2\Psi$ plot is shown in Figure 10; this particular example shows no evidence of the splitting associated with the presence of shear stress.

3.3 Design of Experiment

Three sets of HSLA-100 steels plates were used in this research, all constructed and provided by CDNSWC. The first set, labeled GPX, is a single, as-received plate of base material 4.5 inches square and 0.75 inches thick. Two lines were drawn bisecting the plate parallel and perpendicular to the rolling direction. Transverse and longitudinal residual stresses were measured every one-half inch along these lines; a diagram of these measurement locations is shown in Figure 11. It should be noted that for all diagrams of measurement locations in this document, the circles indicating the measurement locations are approximately proportional to the size of the x-ray beam. XRD determines the average residual stress in all grains irradiated by the x-ray beam.

The second set of plates are weldments processed using the parameters found in Table 3. There are three groups of weldments, each with one changing variable while all others are held constant. The RS-P group consists of five welds with different preheating temperatures varying from 75°F to 400°F. The preheating duration ensured that the entire thickness of the weldment reached a uniform temperature. The RS-T group is a pair of welds of thicknesses ¾ inch and 2 inches. The RS-H group consists of two welds with heat inputs of 35.3 and 50.7 kJ/in. Note that this particular experimental matrix has repetitions; the RS-P2 and RS-T1 welds were prepared identically. This allowed for the determination of the reproducibility of the welding process in terms of the surface residual stress state generated. In addition, these two welds were processed using parameters identical to those of the RS-H group, but with a heat input intermediate between the those of the RS-H1 and RS-H2 weldments, thus creating a total of three welds for the RS-H group.

All x-ray data collected from the weldments were within 11 millimeters of the base of the weld bead. The weldments in the RS- groups were heavily ground perpendicular to the length of the weld bead in preparation of welding. This is standard procedure for bead-on-plate welding in order to create a "clean" surface upon which to put the weld bead.[44] However, because grinding affects

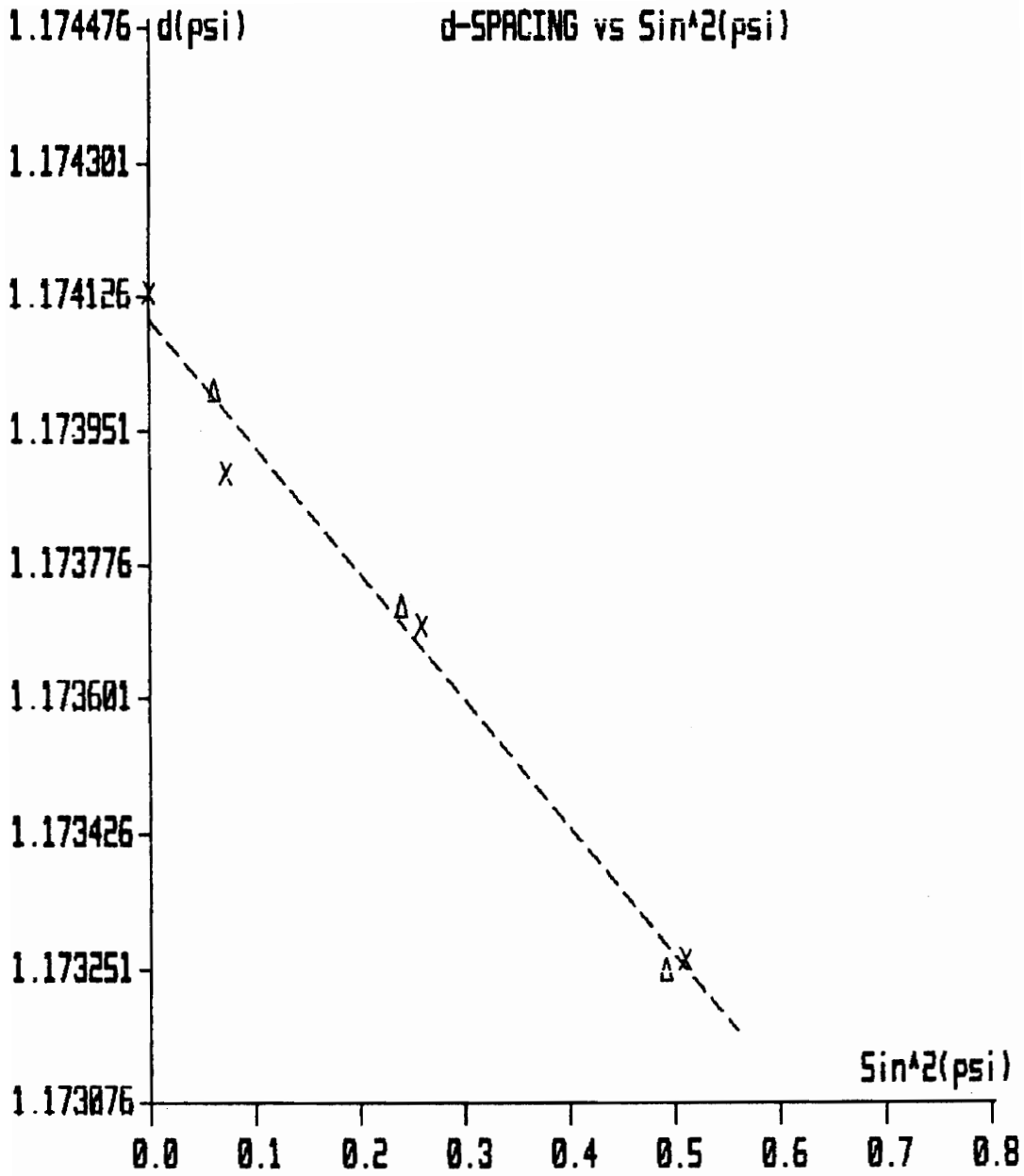

Figure 10. Typical d vs. $\sin^2\psi$ plot without any evidence of shear stress.

Table 3. All samples, including processing parameters, as provided by CDNSWC.

Designation	Welded	Ground	Preheat (°F)	Thickness (in.)	Heat Input (kJ/in)
GPX	no	no	n/a	n/a	n/a
RS-P1	yes	yes	75	0.75	42.7
RS-P2	yes	yes	125	0.75	42.7
RS-P3	yes	yes	225	0.75	42.7
RS-P4	yes	yes	300	0.75	42.7
RS-P5	yes	yes	400	0.75	42.7
RS-T1	yes	yes	125	0.75	42.7
RS-T2	yes	yes	125	2.00	42.7
RS-H1	yes	yes	125	0.75	35.3
RS-P2 (T1)	yes	yes	125	0.75	42.7
RS-H2	yes	yes	125	0.75	50.7
SR-1	no/yes	no	400	0.75	42.7
SR-2	no/yes	no	75	0.75	42.7

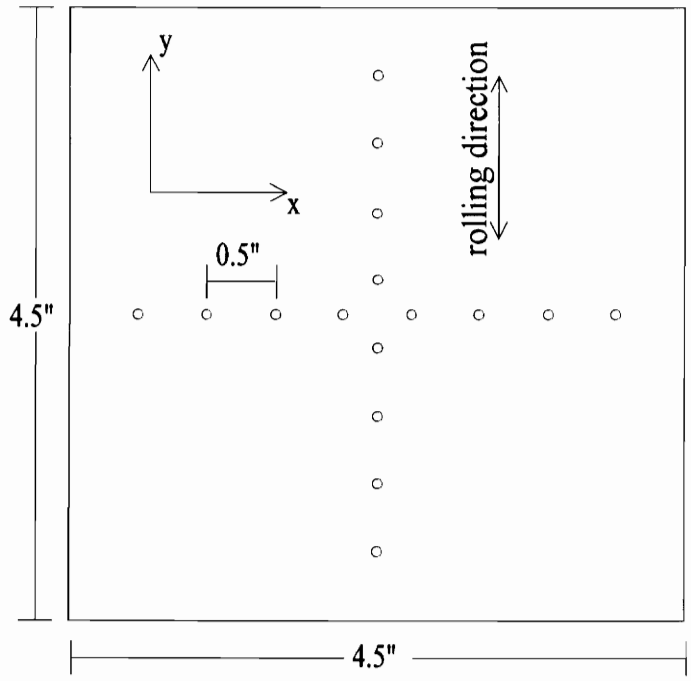

Figure 11. GPX as-received base plate showing dimensions and locations of XRDRS measurements; σ_t is in the x-direction and σ_l is in the y-direction.

the surface residual stress state of the material, this process makes it difficult to determine whether the stresses measured are residual stresses due to welding or residual stresses due to grinding. This led to the construction of a third set of plates which were examined using x-rays.

The third set of plates, each six inches square and 0.75 inches thick and labeled SR-1 and SR-2 (Stress Relieved), were vacuum annealed at 1200°F for one and two hours, respectively. The pre- and post-annealing heating and cooling rates were ≤100°F/hour. X-ray diffraction measurements of residual stress were made at the locations shown in Figure 12 in order to determine the pre-welding surface residual stress state. The two SR- plates were then welded using parameters from the RS- group (SR-1 using RS-P5 welding parameters, and SR-2 using RS-P1 welding parameters), resulting in two pairs of weldments welded in the same manner, differing only in the severe grinding performed on the RS- group welds.

When measuring the bead-on-plate weldments for residual stresses using XRD, the following procedure was used: a point was marked at the weld base, at approximately the midpoint of the length of the weld bead; x-ray residual stress measurements were made on the base material (in both the longitudinal and transverse directions) moving perpendicular from the weld in five two millimeter increments. This created a total of twelve measurements (six in each direction) for one line on one side of the weld bead; the procedure was then repeated on the opposite side of the weld bead (see Figure 13). A micro-positioning stage was used to move the sample the desired increments for all data collection. The distance between the measurement locations was the same as the diameter of the collimators being used. Due to divergence of the x-ray beam, there was some overlap of the areas averaged for residual stress. This was not viewed to be a problem.

On two of the eleven weldments examined (RS-P2 and SR-2), four additional lines of measurements were made, each approximately one inch away from either side of the originals (see Figure 14). This was done in order to examine the variation of the surface residual stress versus distance along the weld bead. Some data points along each line were repeated in order to determine whether the reproducibility of the x-ray diffraction data was significantly different from the counting statistics error to be discussed in Section 4.

A question arises as to whether the x-rays are measuring residual stresses due to welding or residual stresses due to grinding. Photo-macrographs of cross-sections of identically processed weldments reveal heat affected zones that extend 1.2-2.5 millimeters from the base of the weld

bead. Different weldments have different sizes of heat affected zones depending on the thermal effects of the welding process. Verbal discussions between Virginia Tech and the CDNSWC found both parties in agreement that any grinding stresses induced into the material close to the fusion zone were likely to be relieved by the heat of welding. Thus, we assume that the residual stresses measured by XRD within the HAZ are welding residual stresses and not grinding residual stresses. Outside this HAZ, the heat of welding may not be sufficient to anneal the stresses induced by grinding. It should be possible to determine the extent of annealing caused by the heat of welding by comparing the patterns of residual stresses found in the SR- group welds with the identically processed welds in the RS- group. Section 5.2 will discuss this further.

To summarize, we have three sets of HSLA-100 steel plates: the GPX as-received plate which was examined using x-rays to determine the surface residual stress state of the as-received material; the RS- group which was heavily ground before welding, welded using different processing parameters, then measured for surface residual stresses using XRD; and the SR- group which was vacuum annealed, examined using x-rays to determine the pre-welding residual stress state, welded (without grinding) using parameters from the RS- group, then measured for surface residual stresses using XRD. These three sets of plates were selected to allow for the determination of the following with respect to the surface residual stress state: the effect of annealing unwelded plates, the effects of pre-grinding bead-on-plate weldments, and the effect of different welding processing parameters.

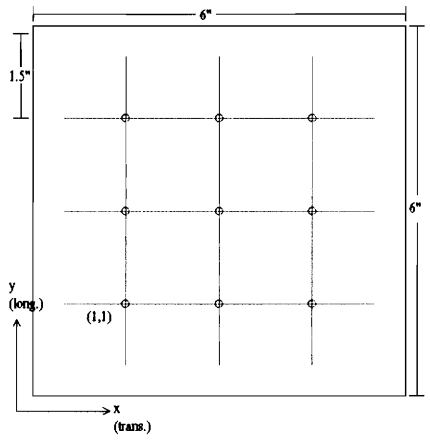

Figure 12. SR- group pre-welding XRDRS measurement locations. Measurements in the x-direction are transverse and measurements in the y-direction are longitudinal to the rolling direction.

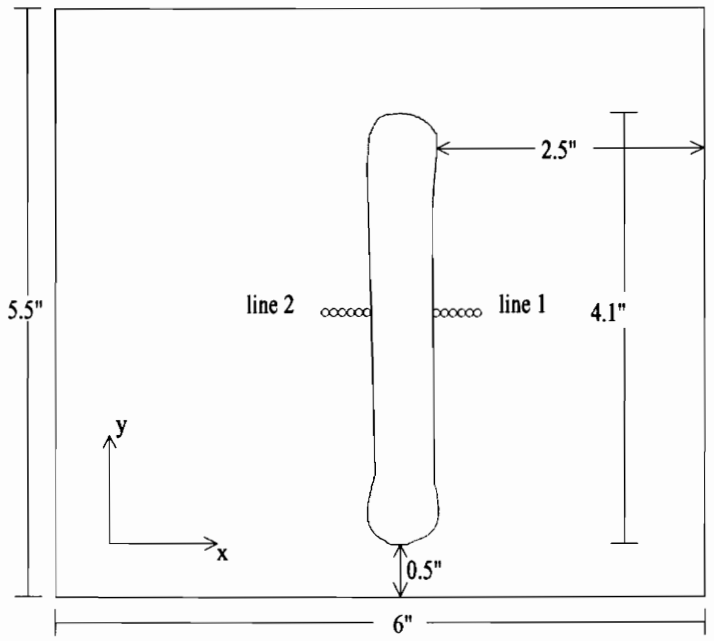

Figure 13. Diagram of XRDRS measurement locations on a bead-on-plate weldment. The circles represent measurement locations for measurements in both the transverse (x) and longitudinal (y) directions.

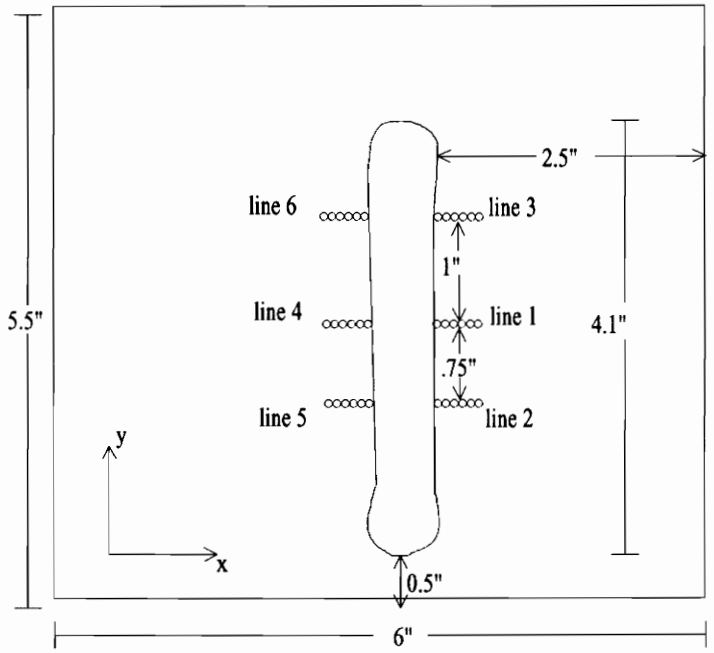

Figure 14. Diagram of XRDRS measurement locations (six lines) on a bead-on-plate weldment. The circles represent measurement locations for measurements in both the transverse (x) and longitudinal (y) directions.

4. REPRODUCIBILITY OF RESIDUAL STRESS DATA

The XRDRS procedure has several possible sources of error, such as alignment, x-ray optics, and statistical errors.[45] These sources of error may be minimized by using careful experimental techniques. However, even when minimized, knowledge of the magnitude of these errors is important for the proper interpretation of the residual stress data. A series of experiments was conducted to quantify these errors as applied to our instrumentation and application. The knowledge gained from this experiment was then extrapolated to the data gathered throughout these investigations, allowing for proper data analysis while taking into consideration error within the XRDRS procedure.

The standard deviation of all the errors inherent to the XRDRS technique (i.e. optical and/or alignment) was designated σ_{ex}, or experimental error. A single random spot on a weldment was repeatedly measured for residual stress without adjusting the PARS system between measurements. Statistical analysis of the resulting data led to $\sigma_{ex} = \pm 1.2$ ksi. Thus, the best possible accuracy that can be expected when measuring residual stresses in our particular case is ± 1.2 ksi.

As was seen in Section 3.3, a large amount of data was gathered in order to achieve the goals of this research. Because the collection of one residual stress data point may require a great length of time, it is imperative that the data collection process be as efficient as possible. However, it is equally important that in reducing the measurement time the statistical accuracy of the experiment is not diminished. Noyan and Cohen derive the error associated with computing the 2θ position of the diffraction peak arising from the random arrival of the x-rays at the detector with respect to time.[46] This error in computing the 2θ value causes an error in the resulting stress, called σ_{cs}, or the counting statistics error. The following equation,

$$\sigma_{cs} \propto t^{-\frac{1}{2}} \tag{11}$$

gives the relationship between the counting statistics error and the measurement time at $\psi=0$, t, for

fixed time measurements as used here. Note that the actual time to acquire a residual stress data point is much greater than t, because there are six other ψ angles and the PARS increases the acquisition time for $\psi \neq 0$ in order to compensate for lower diffracted intensities due to increased absorption for $|\psi| > 0$.

To optimize both of the above competing goals, a second experiment was conducted. Measurements were made on a random location with a two millimeter diameter round collimator. The change in σ_{cs} was observed while the count time at $\psi=0$ was increased incrementally from ten seconds to five minutes (the σ_{cs} is computed by the PARS). These data are plotted in Figure 15; the slope of a line regressed through these data is -0.56 ± 0.03, in near agreement with theory. The discrepancies in the slope may be due to no quantitative account of the noise in the system being taken.

Due to the power law relationship between σ_{cs} and t, and the level of electronic background noise in the position sensitive detector, a point should be reached where an increase in t does not result in an appreciable decrease in σ_{cs}. In this experiment, the desired statistical accuracy was obtained without having to increase the measurement time to the level where the effect of the electronic noise would become noticeable. The above data reveal that a measurement time of 150 seconds (at $\psi=0$) produced a counting statistics error of approximately ± 1.2 ksi. Because $\sigma_{ex} = \pm 1.2$ ksi was the maximum accuracy achievable, any attempt to improve σ_{cs} beyond this would be counterproductive. For all data collected for this thesis, measurement times were chosen to maintain $\sigma_{cs} \leq 1.2$ ksi.

All of the data presented in Figure 15 were acquired using a two millimeter diameter round collimator (the same collimator that was used for measurements longitudinal to the weld bead). As noted in Section 3.3, x-ray measurements in the transverse direction were made using 2x5 millimeter slit collimator. The approximate beam size from the slit, A_s, is 10 mm^2, while the approximate beam size from the round collimator, A_r, is 3.14 mm^2. The counting statistics errors are proportional to the diffracted intensity, and diffracted intensity is proportional to beam size; thus, for the same measurement time, σ_{cs}^{slit} will be lower than σ_{cs}^{round}, allowing for a decrease in t, when acquiring transverse residual stress data, with no increase in σ_{cs}. This usually led to measurements times between 120-150 seconds for longitudinal data and 90-120 seconds for transverse data. The

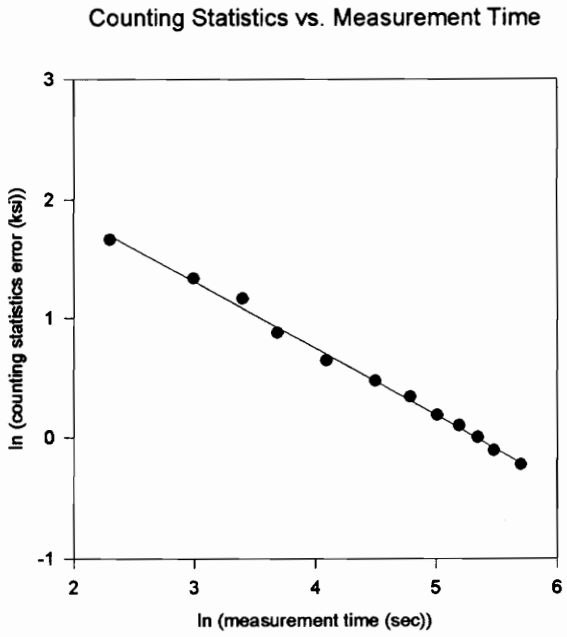

Figure 15. Ln-ln plot of the variation of counting statistics error with measurement time.

intensity of the diffracted beam is affected by the surface condition of the diffracting material, explaining the range of times for measurements in a given direction. For example, the vacuum annealed plates have a very smooth, mirror-like surface which is conducive to x-ray diffraction studies, allowing the measurement time to be decreased with no loss in statistical accuracy.

Another possible source of error is operator error, σ_{op}. Two operators collected the data presented here; by measuring the same locations repeatedly after complete realignment of the sample before each measurement, the operators' ability to position the sample was tested. This is important because in the presence of a stress gradient, a slight misplacement of the sample will result in large variations in the measured residual stress. Analysis of the data generated in such an experiment found $\sigma_{op} = \pm 6$ ksi. The error involved in the positioning of the sample, though small, is significantly greater than the errors caused by either counting statistics or experimental errors ($\sigma_{op} > \sigma_{ex} \geq \sigma_{cs}$). All data reported here will have error bars of ± 6 ksi. It should be reemphasized that the relative values of residual stress are of primary importance, and the accuracy of these values secondarily so. In that case, σ_{ex} might be more appropriate to use as error bars, but σ_{op} shall be used for a more conservative interpretation of the resulting data.

Also of concern is the reproducibility of the welding process with respect to the surface residual stress state generated. The RS-T1 and RS-P2 plates were processed identically in order to address this concern. The XRDRS results from these two plates are shown in Figure 16 and Figure 17. The x-axis error bars in these and the following figures, ±1 mm, are equal to half of the diameter of the collimator being used. This provides for better visual interpretation of the area over which surface residual stresses were averaged. The vertical lines representing the edge of the HAZ were determined from macrographs of cross-sections of an identically processed set of weldments. These photographs, and the HAZ itself will be discussed further in Section 5.2.

Examination of the transverse residual stress state reveals no statistically significantly difference within the HAZ of two welds processed identically. Outside of the HAZ, the stresses are not as uniform, but this may be attributed to the non-uniform grinding which took place on both plates before welding. The grinding is a manual process, and subject to large variation at the discretion of the operator. This variation is noticeable when examining the direction and depth of the grinding scars present on all of the RS- group weldments. For the longitudinal direction, stresses are similar, but do show statistically significant differences. However, these differences are only 30-40 ksi, and may also be attributed to grinding. This grinding will make it very difficult to determine whether any trends observed outside of the HAZ are due to the welding process or the grinding. The effects of grinding will be discussed more extensively in Section 5.3.

Also of concern is the variation of the surface residual stress state in the base material at different locations along the weld bead. It is known that there are end effects during the development of residual stresses related to the moving heat source associated with welding.[47,48] In order to determine the extent of these end effects on the weldments examined in this research, additional lines of measurements were made on two welds, as was shown in Figure 14. These six lines allow for the examination of the residual stresses surrounding the middle 43% of the length of the weld bead. The resulting data are shown in Appendix A and are plotted in Figure 18. The averages and standard deviations of the data at each measurement location are shown in Table 4. The transverse and longitudinal measurements made on the SR-2 weldment for the most part reveal less of a statistically significant difference than σ_{op}= ±6. The surface stress state also appears to be symmetrical about the weld bead. The six lines from the RS-P2 weldment show larger statistically significant differences, anywhere from ±2-36 ksi. When comparing the RS-P2 data to the SR-2 data, the

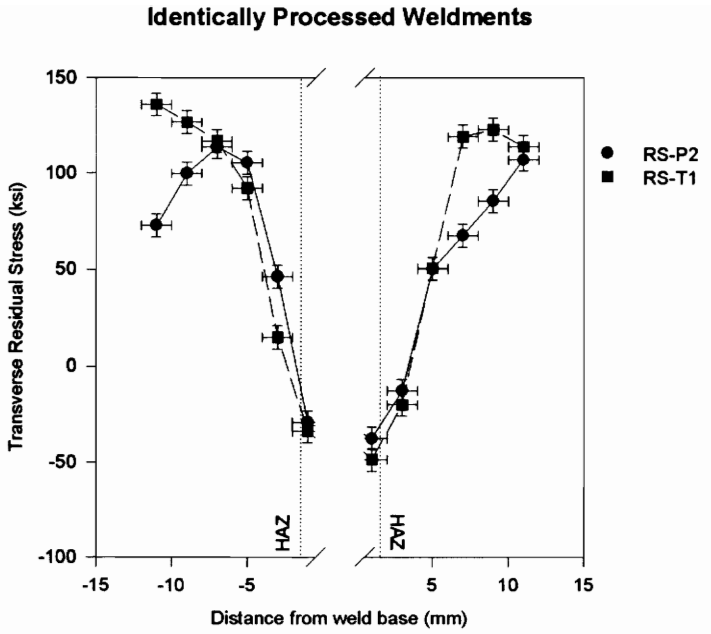

Figure 16. Reproducibility of the welding process with respect to σ_t (RS-T1 vs. RS-P2).

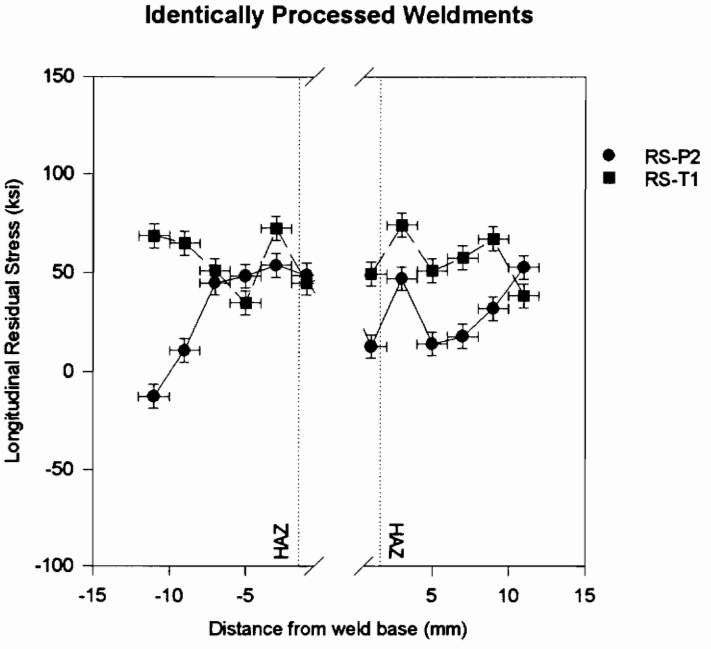

Figure 17. Reproducibility of the welding process with respect to σ_l (RS-T1 vs. RS-P2).

Table 4. Averages and standard deviations of SR-2 and RS-P2 residual stress data at each measurement location.

	SR-2				RS-P2			
	σ_t (ksi)		σ_l (ksi)		σ_t (ksi)		σ_l (ksi)	
Distance	Average	St. Dev.	Average	St. Dev.	Average	St. Dev.	Average	St. Dev.
-11 mm	-12.2	3.9	-55.9	5.0	31.5	36.1	-12.4	
-9 mm	-0.2	7.3	-43.4	11.8	88.2	10.1	14.9	11.2
-7 mm	1.1	5.7	-30.3	10.3	100.1	12.7	31.0	12.6
-5 mm	-0.3	4.2	-8.7	16.6	94.1	12.3	39.9	8.3
-3 mm	-2.5	2.5	49.5	21.3	49.6	3.9	54.7	9.9
-1 mm	-23.1	2.7	60.6	8.5	-27.5	2.0	49.6	4.3
1 mm	-20.8	11.4	44.4	9.0	-34.9	6.5	39.4	23.5
3 mm	-2.9	10.0	46.6	17.9	27.2	35.8	52.2	6.2
5 mm	-5.1	3.9	3.2	10.8	90.2	34.8	38.8	21.3
7 mm	-7.7	2.2	-29.1	2.9	96.7	26.6	29.0	16.2
9 mm	-8.6	3.6	-41.2	3.2	106.5	23.5	27.9	4.8
11 mm	-13.8	2.3	-48.4	0.9	111.9	8.1	39.8	25.1
	Avg. SD	4.98	Avg. SD	9.85	Avg. SD	17.69	Avg. SD	13.04

grinding which took place on the RS- group must be taken into account. Not only is the grinding different from plate to plate, but the grinding also varies over different locations on the same weldment, as is shown when comparing the data in Table 4. However, the variation along the length of the RS-P2 weldment is not so great as to necessitate more than one measurement line across the middle of the length of the weld bead.

From the above discussion, we may conclude that:

- the maximum accuracy of our experimental method is ±6 ksi, which is larger than the errors inherent to the experimental apparatus,
- the welding process is reproducible with respect to the surface residual stress state generated,
- the variation of the residual stresses around the bead of a bead-on-plate weldment is such that only one measurement line across the middle of the weld is needed to gain an understanding of the stress state, and
- the averages of the variations of the residual stress along different lines of measurements on an unground sample are ±4.98 (σ_t) and 9.85 ksi (σ_l), and are much less than the same data for a ground sample, ±17.69 (σ_t) and 13.04 ksi (σ_l).

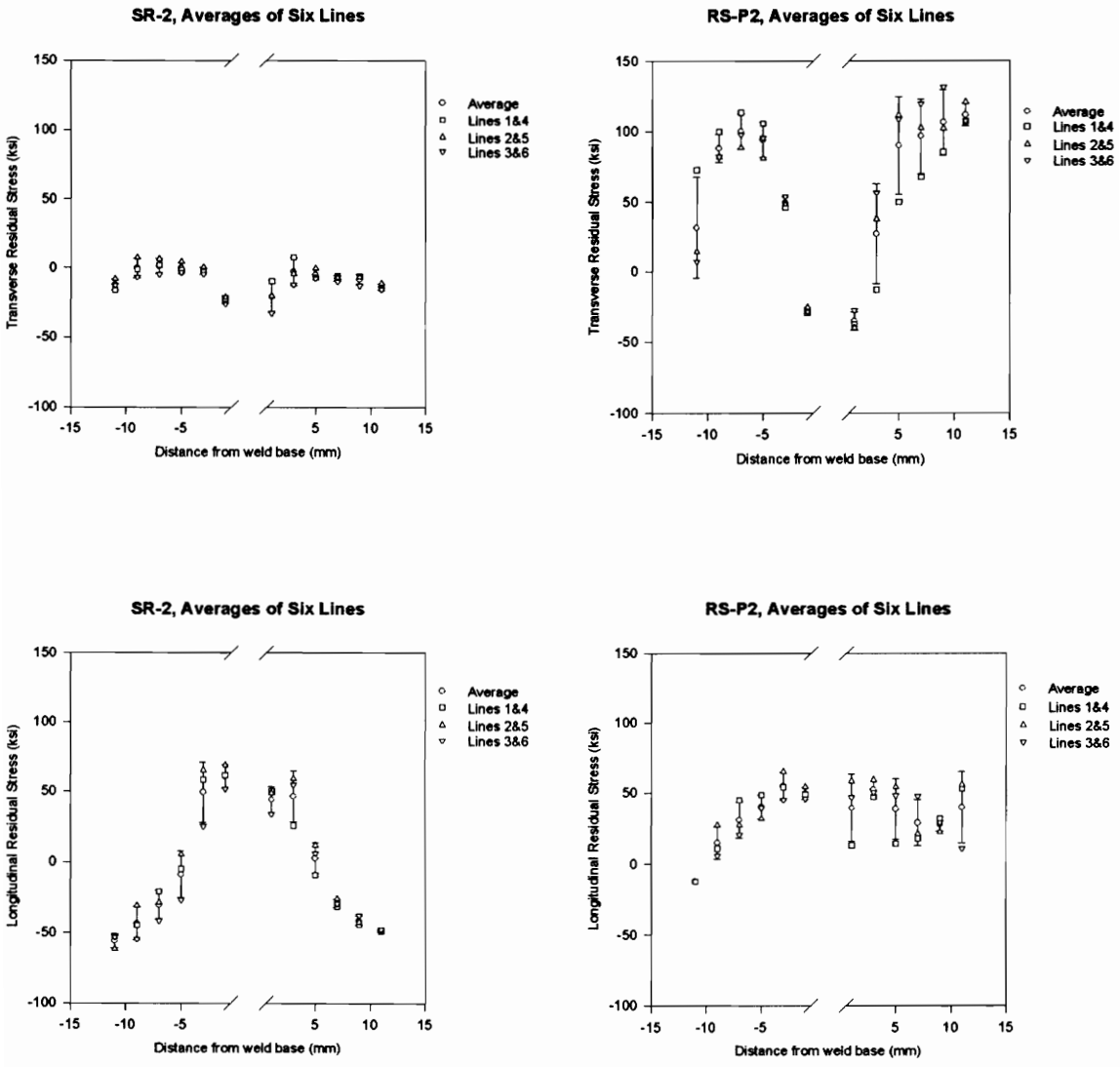

Figure 18. RS-P2 and SR-2, all six lines including error bars representing the standard deviations.

5. RESULTS AND DISCUSSION

5.1 Residual Stresses in Unwelded Plates

X-rays were used to determine the surface residual stress state of a sample of as-received, HSLA-100 base material following the procedure described in Section 3.3. These results are shown in Table 5. A large portion of the surface of the plate is extensively corroded, and these locations are accounted for by the "n/a" values in the table. This oxide scale makes it impossible to measure residual stress using XRD without some sort of surface preparation (i.e. electropolishing or chemical etching). A statistical test reveals that the data for the four lines of measurements cannot be considered unequal. Knowledge about the number of points measured and the population standard deviation of the residual stress at different locations on the plate leads to a 95% confidence that the average of the data for the entire plate is within ±3.5 ksi of the true average of the residual stress state. All residual stresses are compressive, and each set remains relatively consistent across the length of the measurement line. A simple statistical test of the equality of the means shows that the averages of the four sets of data cannot be considered unequal; i.e., there is no difference between residual stresses parallel to and perpendicular to the rolling direction.

In order to determine the effect of vacuum annealing unwelded HSLA-100 base material, the SR- group welds were heat treated as described in Section 3.3. The two plates were examined for pre-welding residual stresses according to the procedure described in that same section. The data for both plates can be found in Table 6. A paired samples t-test conducted on the two blocks of data results in no statistically significant difference between the surface residual stress state of a plate vacuum annealed at 1200°F for one hour and another plate undergoing the same heat treatment for twice the length of time. In addition, there is no statistically significant difference between the residual stress state of the GPX as-received plate and the vacuum annealed plates. The standard deviations of the data collected from the three plates decrease with increased annealing time; it

Table 5. GPX as-received base plate residual stress data, including statistics to compare the different groups. The "n/a" values indicate areas where corrosion made XRDRS impossible.

	X-line		Y-line	
Distance from edge	σ_l (ksi)	σ_t (ksi)	σ_l (ksi)	σ_t (ksi)
0.5"	-24.4	-4.7	n/a	n/a
1.0"	-19.5	-17.8	n/a	n/a
1.5"	-25.2	-31.6	-16.9	-32.4
2.0"	-13.6	-2.8	-10.6	-28.2
2.5"	-21.9	-14.4	-14.7	-30.2
3.0"	n/a	n/a	-10.0	-20.6
3.5"	-10.3	-15.5	-8.9	-19.8
4.0"	n/a	n/a	-18.2	-15.7
Average	-19.2	-14.5	-13.2	-24.5
Std. Dev.	6.0	10.4	3.9	6.7

Table 6. SR- group, pre-welding residual stresses, including statistics to compare the different groups.

SR-1					SR-2				
	Top face		Bottom face			Top face		Bottom face	
	σ_l (ksi)	σ_t (ksi)	σ_l (ksi)	σ_t (ksi)		σ_l (ksi)	σ_t (ksi)	σ_l (ksi)	σ_t (ksi)
(1,1)	-12.5	-17.1	-21.6	-16.2	(1,1)	-15.5	-17.3	-13.2	-9.5
(1,2)	-9.7	-15.1	-16.7	-11.1	(1,2)	-15.4	-19.7	-13.2	-12.3
(1,3)	-11.8	-21.3	-11.1	-7.1	(1,3)	-20.0	-23.8	-17.0	-18.1
(2,1)	-7.0	-12.0	-19.5	-9.3	(2,1)	-10.3	-14.2	-14.2	-13.1
(2,2)	-10.3	-15.0	-19.0	-18.3	(2,2)	-19.0	-18.2	-13.9	-13.0
(2,3)	-18.1	-14.3	-14.6	-8.4	(2,3)	-14.4	-13.8	-12.6	-11.4
(3,1)	-10.3	-13.4	-17.6	-12.9	(3,1)	-15.1	-15.0	-13.8	-13.1
(3,2)	-4.2	-12.3	-20.9	-14.1	(3,2)	-14.5	-16.7	-13.3	-10.1
(3,3)	-13.5	-16.8	-11.3	-6.4	(3,3)	-13.5	-18.2	-18.4	-15.1
Avg.	-10.8	-15.3	-16.9	-11.5	Avg.	-15.3	-17.4	-14.4	-12.9
St. Dev.	3.9	2.9	3.9	4.1	St. Dev.	2.9	3.1	2.0	2.6
Total: SR-1					Total: SR-2				
Avg.			-13.6		Avg.			-15.0	
St. Dev.			4.4		St. Dev.			3.1	

appears that vacuum annealing, while not significantly changing the surface residual stresses, does reduce the variation in the stress states.

The examination of these three unwelded, HSLA-100 base plates leads to the conclusion that the average surface residual stress state of unwelded HSLA-100 base plate is approximately -15.2 ± 5.4 ksi, and this variation is less than the conservative σ_{op}= ±6 ksi derived in Section 4.

5.2 Heat Affected Zone

In Section 3.3, the assumption was made that within the HAZ, the heat associated with welding would relieve any residual stresses induced by pre-grinding the weld base material. In order to apply this assumption, specific information regarding the size of the heat affected zones of the differently processed weldments was required. The microstructure of simulated heat affected zones of HSLA-100 steel was reported to be large packets of lath martensite with interlath films of retained austenite. Both the size of the martensite packet (≈50 μm in diameter) and the amount of retained austenite were found to be larger in the simulated HAZ than in the base metal.[49]

CDNSWC constructed a set of welds identical to the RS- group examined at Virginia Tech. This twin set was sectioned, and the weld bead area was examined metallographically. Photographs were taken of the macrostructure, and these photographs were provided to Virginia Tech so that the size of the HAZ could be determined. It was assumed that identically processed weldments will have heat affected zones of comparable size. A schematic diagram of a weldment cross-section, including locations at which the sizes of the heat affected zones were measured, and a sample macrograph are shown Figure 19. The HAZ measurements of the twin set of plates are shown in Table 7.

If the cross-sectional area of the HAZ is assumed to be ½ the area of an ellipse, the effect of different processing parameters on the size of the HAZ may be determined. The major axis of the HAZ ellipse, a, is equal to ½[Bead+HAZ(l)+HAZ(r)]; the minor axis, b, is equal to the depth. For the RS-P group, increasing preheat temperature increased the size of the HAZ in a linear manner, as shown in Figure 20. This trend is to be expected, because when the base material is at an elevated temperature, it is more likely to be affected by the heat of welding. Another note of interest is that the ratio of the major axis to the minor axis of the HAZ ellipse decreased with increasing preheat temperature (see Figure 21), indicating that as the preheat temperature increased, the depth

Table 7. Size of HAZ of RS- group twin weldments.

Weld	Bead	HAZ (l)	HAZ (r)	Depth
RS-P1	16.1 mm	1.3 mm	1.3 mm	5.0 mm
RS-P2	17.0 mm	1.5 mm	1.5 mm	5.5 mm
RS-P3	17.7 mm	1.7 mm	2.0 mm	6.0 mm
RS-P4	17.3 mm	2.0 mm	2.2 mm	6.0 mm
RS-P5	18.6 mm	2.1 mm	2.3 mm	7.5 mm
RS-H1	16.0 mm	1.5 mm	1.5 mm	5.3 mm
RS-H2	18.5 mm	1.7 mm	2.0 mm	6.2 mm
RS-T2	18.0 mm	1.7 mm	2.3 mm	6.0 mm

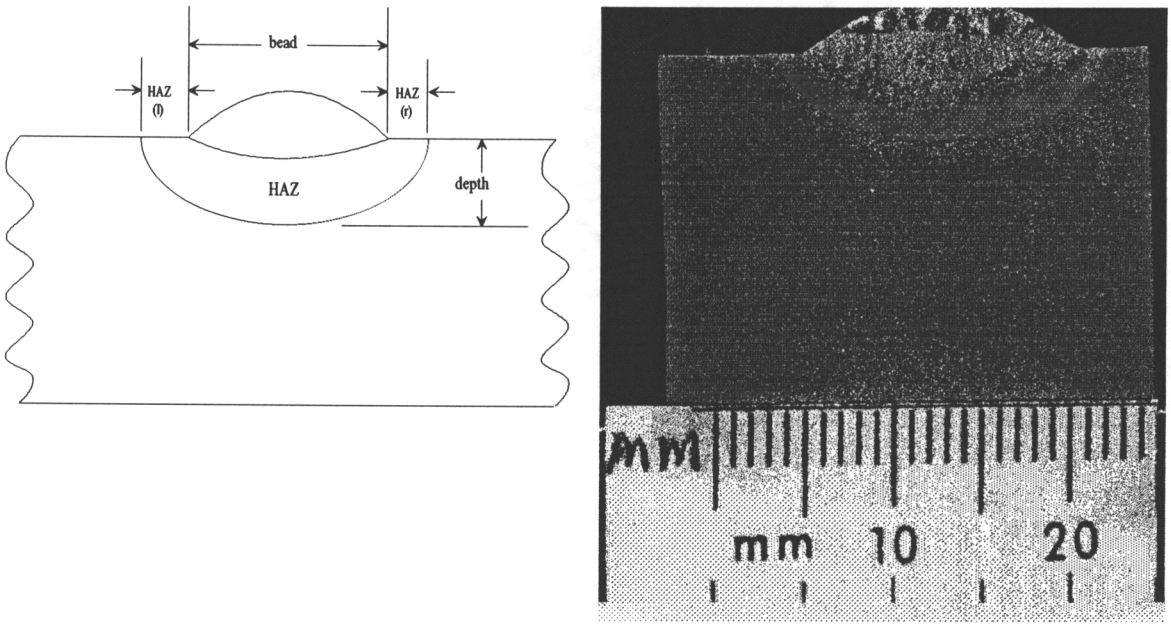

Figure 19. Schematic diagram and macrograph of cross-section of a bead-on-plate weldment.

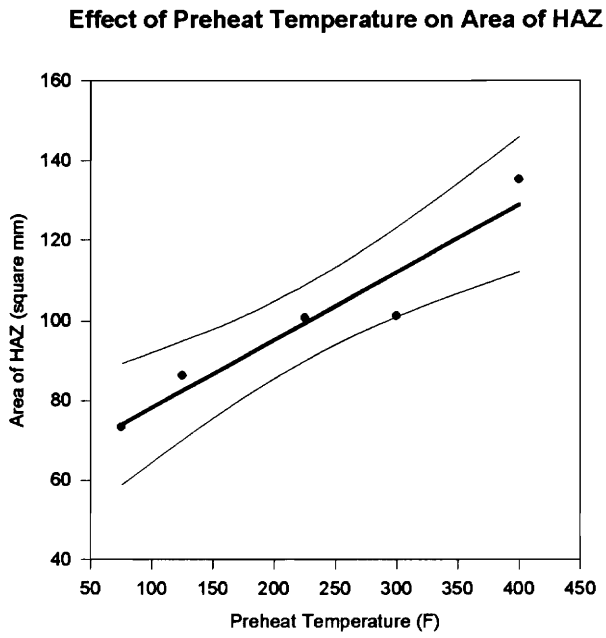

Figure 20. Effect of preheat temperature on the area of the HAZ, including linear regression with 95% confidence interval.

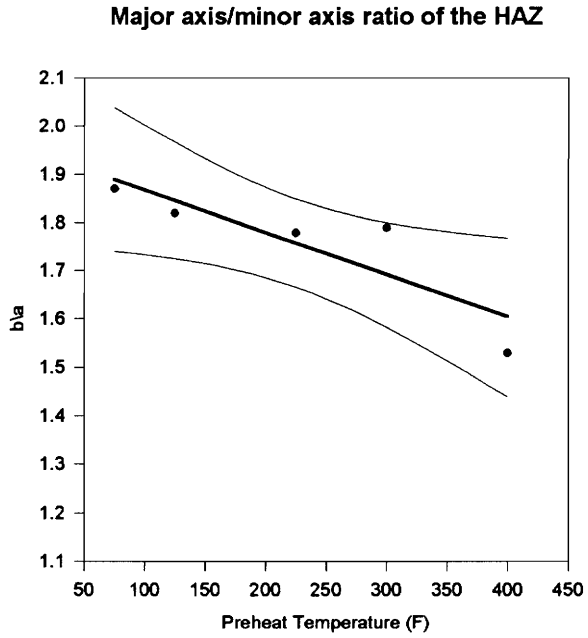

Figure 21. Effect of preheat temperature on the ratio of the major axis to the minor axis of the HAZ ellipse, including linear regression with 95% confidence interval.

of the HAZ increased faster than the width.

Figure 22 demonstrates the effect of increasing heat input with respect to the area of the HAZ. As expected, as larger heat input increases the size of the HAZ. Figure 23 shows the effect of weldment thickness on the size of the HAZ. For identical welding parameters, a two-inch thick weldment has a larger HAZ than a ¾-inch thick weldment. However, any conclusions should be warily drawn due to the small sample size

Examination of the widths of the HAZ on either side of the weld bead makes it clear that only the measurement locations closest to the weld bead have the possibility of being solely representative of residual stresses due to welding. The data taken at x=1 mm averages the residual stress over a 2 mm range, beginning at the base of the weld bead. Note that the length of the HAZ does not always extend across the entire 2 mm; however, at no time does less than 65% of the averaged stress come from the surface of the HAZ. Table 7 shows that the maximum width of the HAZ is 2.3 mm. In those cases where the HAZ does extend beyond 2 mm, the small percentage of the residual stress average that would be from the heat affected area (15%) made it unwise to include such data as residual stress caused by the welding process. Thus, only the data closest to the weld bead may be used when comparing the effects of the different welding parameters on the residual stress state generated.

From these results, the following conclusions may be drawn:

- increasing preheat increases the cross-sectional area of the HAZ,
- as the preheat temperature increases, the depth of the HAZ increases faster than the width,
- increasing heat input increases the cross-sectional area of the HAZ,
- a 2-inch thick weldment has a larger HAZ than a ¾-inch thick weldment,
- when determining the effects of different welding parameters on the residual stress state, only the data closest to the weld bead has the possibility of being considered free of the effects of grinding.

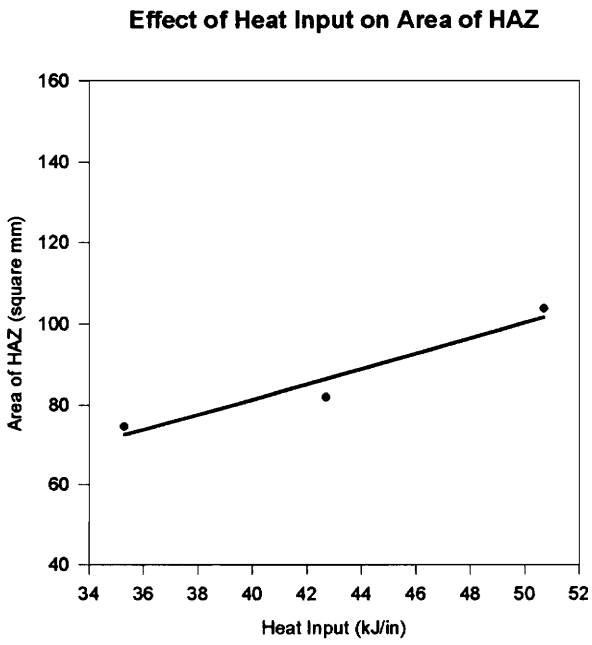

Figure 22. Effect of heat input on the area of the HAZ, including regression.

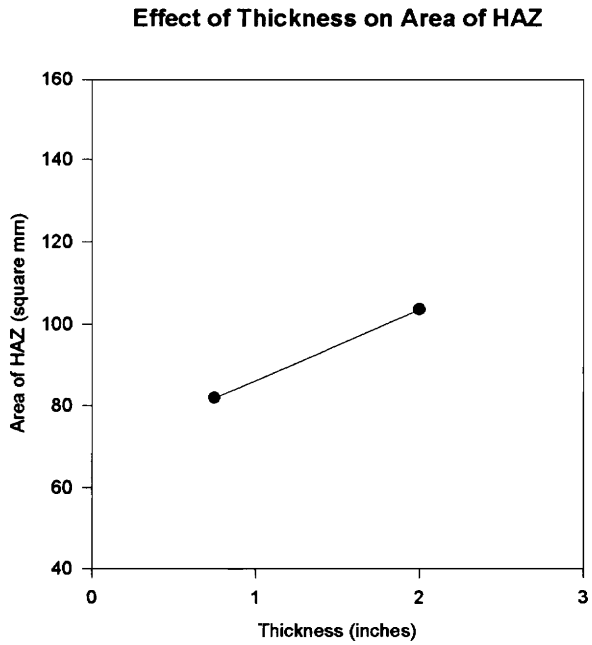

Figure 23. Effect of plate thickness on the area of the HAZ.

5.3 Effects of Grinding

It is well established that grinding has a large effect on both the surface and sub-surface residual stress states.[50,51,52] In some cases, abusive grinding can induce residual stresses of up to 200 ksi between 10-20 μm below the surface.[53] These stresses may react with the heat of welding to create a final residual stress state very unlike that created exclusively by the welding process or exclusively by the grinding process. In order to achieve the goals of this research, the effects of pre-grinding the base plate of bead-on-plate weldments must be isolated. To help accomplish this, the SR- group was processed according to the procedure in Section 3.3, resulting in two pairs of plates processed identically discounting the severe, non-uniform grinding which took place on the RS- group plates before welding.

The data collected from these two pairs of weldments are plotted in Figure 24. It is immediately apparent that grinding significantly changes the magnitude and even the sign of the surface residual stresses. At a preheat temperature of 75°F, grinding increases σ_t outside the HAZ by as much as 115 ksi, turning what is possibly a beneficial, neutral-to-compressive stress state into a highly tensile stress state. There is also a large stress gradient close to the weld bead which did not exist on the unground plates. Longitudinal residual stress patterns are similar in shape but not in magnitude, to the ground sample again having higher stresses by as much as 90 ksi.

The pair of welds preheated at 400°F show similar effects due to grinding: σ_t increases by as much as 115 ksi outside the HAZ in ground samples, again with a large stress gradient that was not present on the unground plate. The stress distribution here is different in both magnitude and shape from the unground weld. Longitudinal data for the same pair show similar patterns with a difference in magnitude of up to 135 ksi. From these observations, it appears that grinding affects the magnitude of the residual stresses in the longitudinal direction, and the magnitude and pattern of the stresses in the transverse direction.

If we assume the simplest case, that grinding stresses and welding stresses are linearly additive, then subtracting the data for the SR- plates from that of the RS- plates will help us isolate the effect of grinding with respect to identically processed weldments. These results are plotted in Figure 25. As expected, the effect of grinding increases as the distance from the fusion zone increases. Note also that similar patterns of differences exist each direction (transverse or longitudi-

nal), while the two directions are less similar to each other. This leads to the conclusion that the grinding process affects the residual stresses directionally.[54]

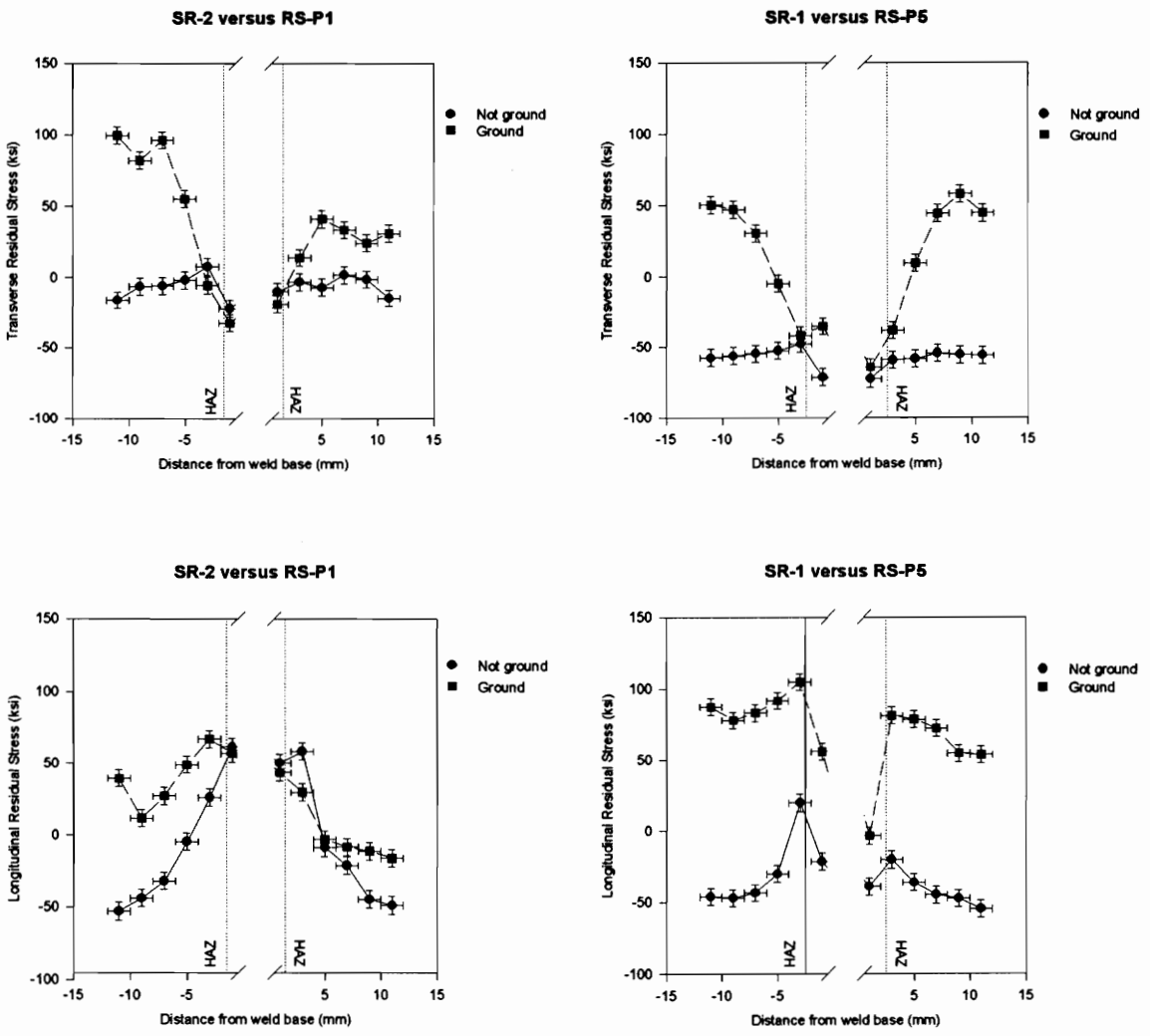

Figure 24. Comparison of identically processed, ground and unground plates.

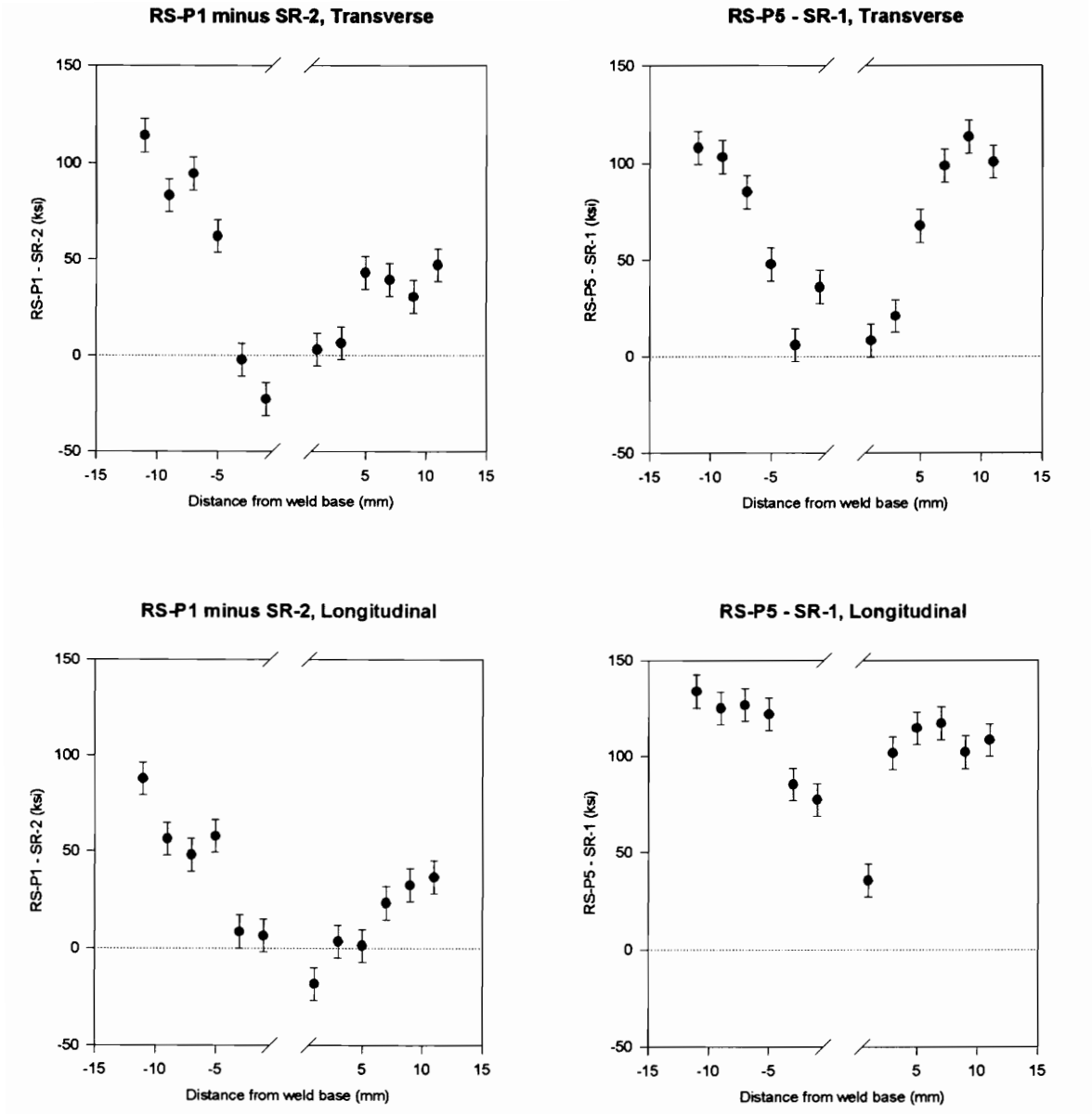

Figure 25. Isolation of the residual stresses due to grinding.

From these results, the following conclusions may be drawn:

- grinding has a significant effect on the magnitude and sign of residual stresses in weldments,
- this effect is directional, and
- the effect of grinding increases as the distance from the fusion zone increases.

5.4 Effects of Processing Parameters on Residual Stresses

In this section, the effects of preheat temperature, heat input, and weld plate thickness will be discussed in terms of the residual stress state generated in the bead-on-plate weldments. Section 5.2 explained why only the set of data closest to the weld bead can be considered purely residual stresses due to welding, even though data were collected up to 11 mm away from the weld bead. All residual stresses outside of the HAZ will be a combination of residual stresses caused by welding and grinding. Any attempt to analyze data outside of the HAZ must take into account the severity and non-uniformity of the grinding which took place on the surface of all RS- group weldments before welding.

In steels, residual stresses are usually a result of tensile shrinkage stresses and compressive transformation stresses.[55] Shrinkage residual stresses result from differences in the cooling rates of differently heated areas. The last material to cool is in tension because it is restrained by the surrounding, already cooled, material. A phase transformation with accompanying volume expansion will induce compressive residual stresses in the transformed material due to restraint by the surrounding, untransformed material. If temperature gradients between the surface of the material and the core result in plastic flow, quenching stresses may arise.[56] Initially, the surface is in tension and the interior is in compression; but after the surface is cooled, the interior continues to cool and thus draws the surface into compression. Because of the temperature difference between the surface and the core of the material, it is also possible to get transformation stresses due to quenching. The final residual stress state generated in a weldment is usually a combination of the above three stress generation mechanisms, though residual stresses due to quenching are, in most cases, not believed to be a noticeable factor.[57] The dominating mechanism(s) will determine the sign of the stress, while all three may contribute to the magnitude.

Preheat Temperature

All data within the HAZ (assumed to be solely residual stress due to welding) were isolated; Figure 26 plots both σ_t and σ_l at the base of the weld bead versus the preheat temperature. The relationship between preheat and residual stress appears to be a linear one over the range of temperatures studied; while the magnitudes of σ_t and σ_l are different, the slopes of the regression lines through each set of data are approximately equal, -0.0716 for σ_t and -0.0731 for σ_l. Increas-

ing the preheat temperature decreases σ_t and σ_l at the same rate. As was stated in Section 2.2, preheating a structure before welding allows the entire thickness to reach a uniform temperature. Upon cooling after welding, stresses induced by shrinking stop increasing when the preheat temperature is reached. When the weldment is cooling, shrinkage causes tensile stresses. Upon reaching the austenite transformation temperature, compressive stresses begin to form due to the volume expansion which takes place. When the transformation is complete, shrinkage again induces tensile stresses. Increasing the preheat temperature decreases (or eliminates) the additional tensile stresses that form after the austenite phase transformation, resulting in a less tensile or more compressive residual stress state after welding.

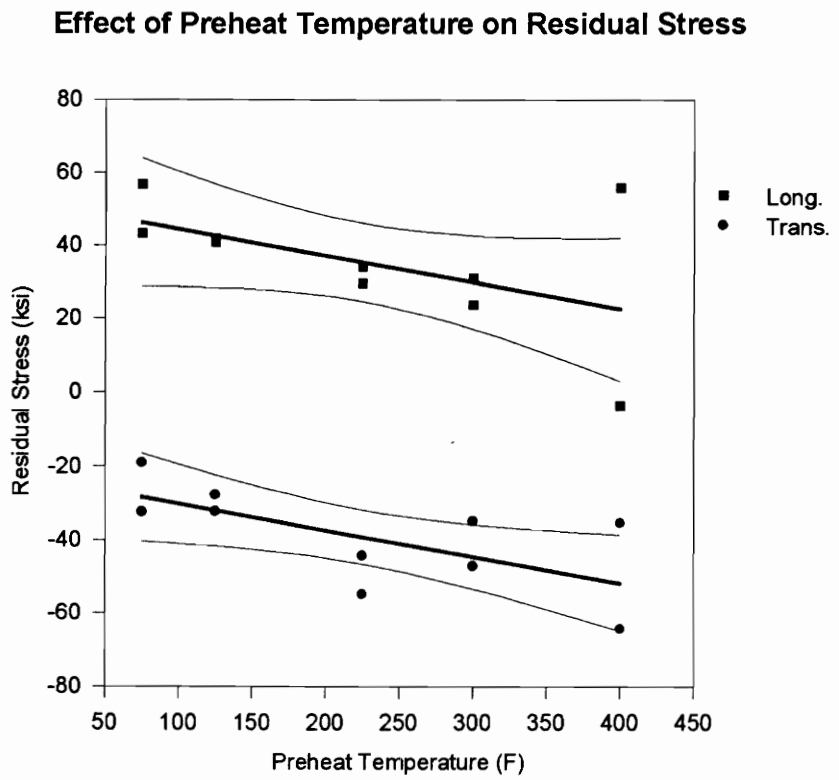

Figure 26. Effect of preheat temperature on σ_t and σ_l, including linear regression and 95% confidence interval.

This effect is most noticeable in the SR- group weldments. Because the SR- group plates were not ground before welding, it is possible to compare the effects of different preheating temperatures on the residual stress state generated. The resulting data is shown in Figure 27. It is apparent that increasing the preheat temperature from 75°F to 400°F makes the residual stress state more compressive. In the transverse direction, the entire residual stress pattern was shifted by approximately -50 ksi. In the longitudinal direction, the higher preheat temperature created more compressive residual stresses in the HAZ, but outside the HAZ the stresses are very similar. This increase in the compressive nature of the stress can be attributed to the increased preheat temperature minimizing tensile shrinkage stresses which are created after the austenite phase transformation.

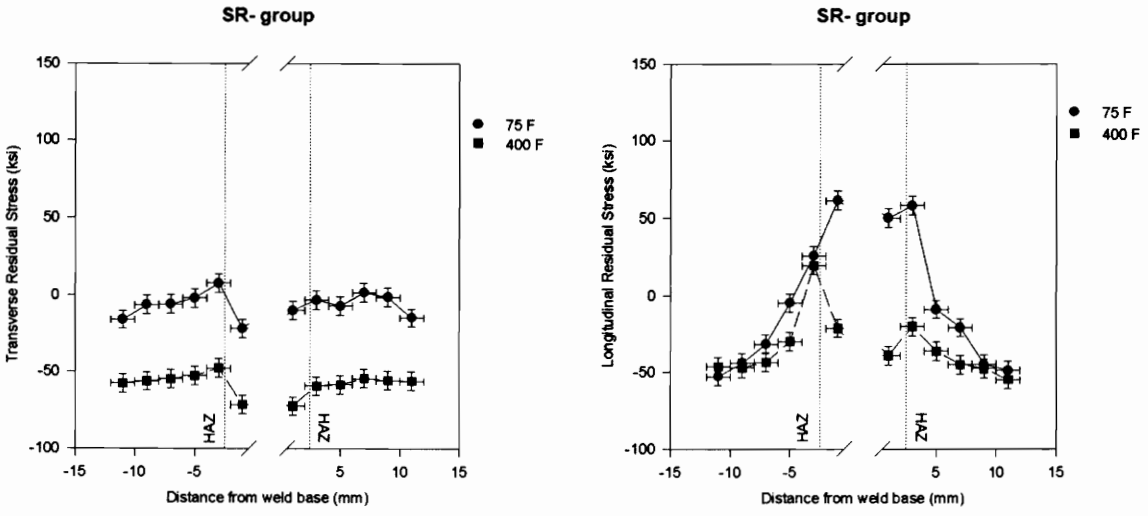

Figure 27. SR- group (not ground) residual stress data.

Heat Input

The effect of heat input on welding residual stresses is shown in Figure 28. It is difficult to determine any possible relationship between the heat input and the resulting residual stress because of the small number of data points. Others have studied this same effect over a range of heat inputs from 7.3-50.3 kJ/in, and reported that increasing the heat input increases the size of the weld seam and thus the size of the HAZ.[58] This induces a slower cooling rate, raises the austenite transformation temperature, and thus leads to an increase of tensile shrinkage stresses in the weld seam after completion of the γ-transformation. Because we are examining such a small segment of the overall stress population (the area at the base of the weld bead) and the range of heat inputs is also small, it is possible that increasing the heat input makes the overall residual stress state more tensile; however, no statistically significant trend is witnessed in the region from which these data were gathered.

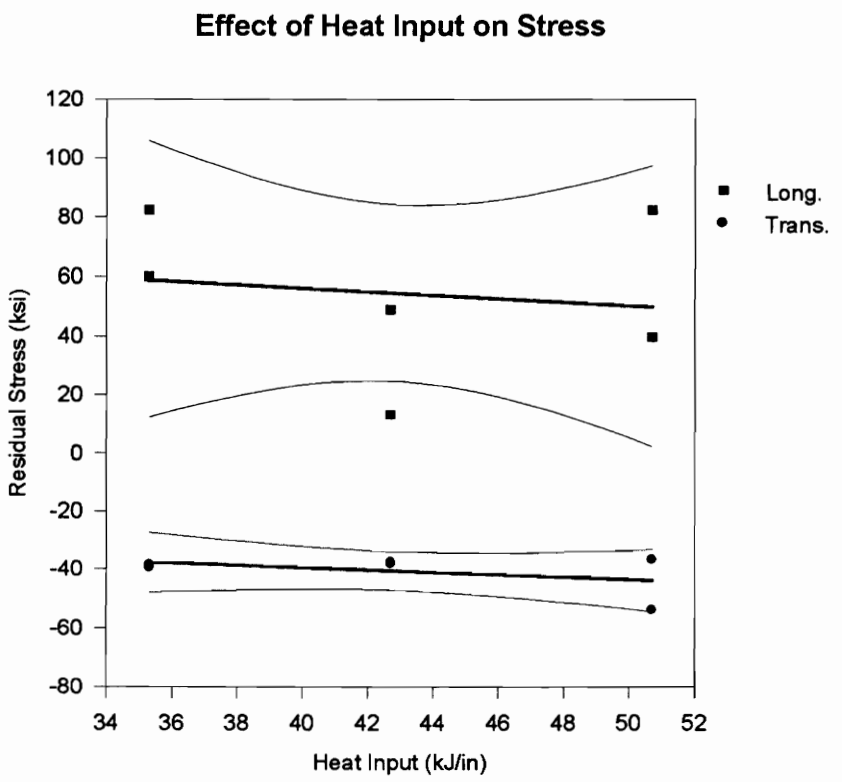

Figure 28. Effect of heat input on residual stress, including regression and 95% confidence interval.

Thickness

Examining the thickness data only within the HAZ (Figure 29) shows opposite trends for the two measurement directions. The σ_l increases with an increase in the base plate thickness from 0.75 to 2 inches, while σ_t decreases over the same change. However, because of the small sample size, it is difficult to draw appropriate conclusions.

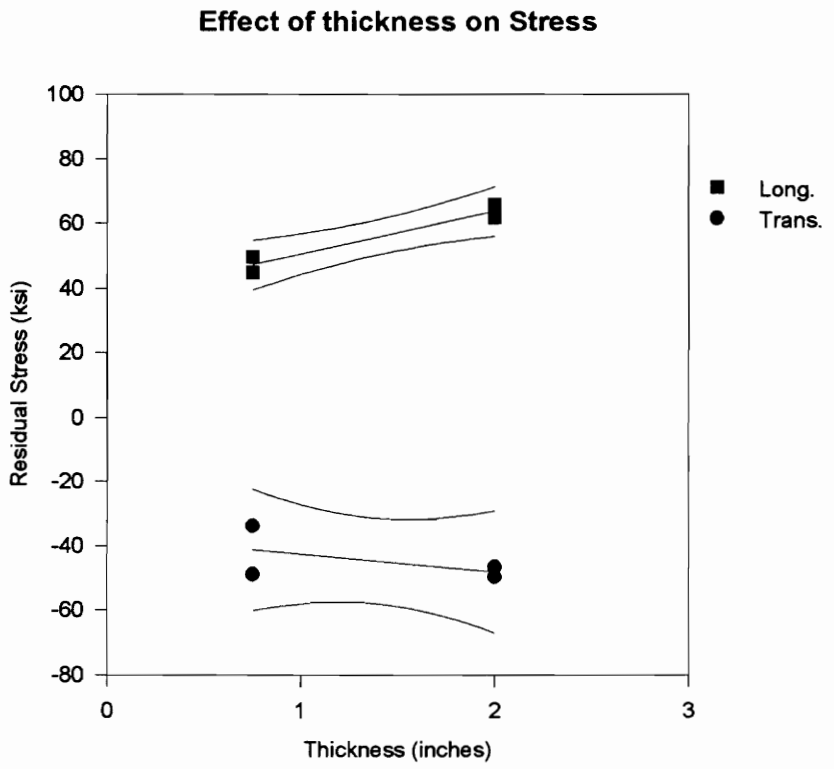

Figure 29. Effect of plate thickness on welding residual stresses, including linear regression and 95% confidence interval.

5.5 Residual Stresses Outside the HAZ

When comparing RS- group data over the entire measurement range, each direction shows a distinct pattern. Transverse residual stresses are always compressive at the base of weld bead, and quickly become tensile as the distance from the weld base increases. These tensile residual stresses sometimes approach the yield strength of the material. Longitudinal residual stresses are always tensile at the base of the weld bead, and slowly decrease as the distance from the weld base increases. When examining longitudinal data, note the residual stress peak just outside of the HAZ; this tensile peak is the result of transformation stresses, as was explained in Section 2.2. In the longitudinal direction, the material just outside of the transforming zone is placed in tension by the expanding transforming region.

Figure 30-Figure 35 show σ_t and σ_l, respectively, for all of the RS- group weldments. Utilization of nonparametric statistics did not reveal any consistent trend of residual stress with respect to the different processing parameters over the entire area studied. However, the small number of data points to compare at each distance limits the power of any statistical procedure, making it difficult to use any statistical analysis tools in an attempt to detect any possible trends among the data.

Figure 36 plots the residual stresses at 11 mm from the weld bead versus preheat temperature. The linear relationship between stress and preheat which exists at the base of the weld bead is not apparent here. This leads to the assumption that the stresses due to grinding dominate the residual stress state of a ground and welded plate. In addition, the severe, non-uniform grinding may effect the residual stress state in different areas of the weld plate differently. This makes it impossible to distinguish between effects of welding parameters and the effects of grinding on the residual stress state outside the HAZ.

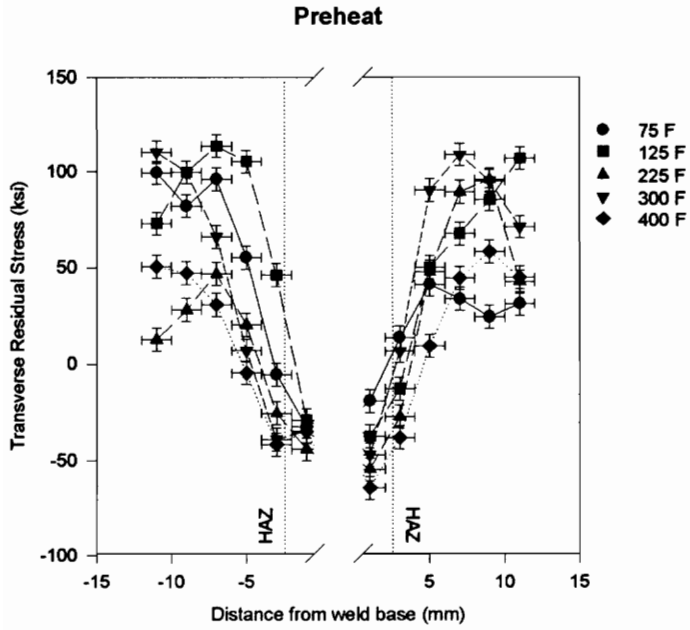

Figure 30. RS-P group σ_t data.

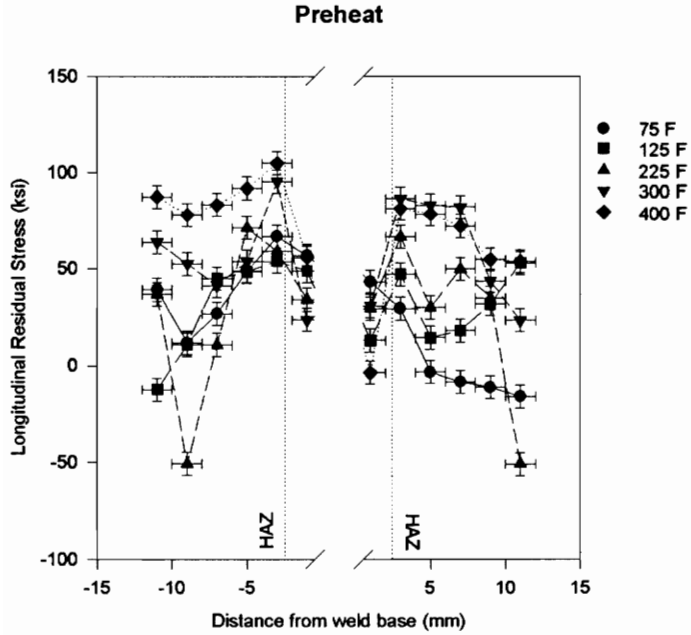

Figure 31. RS-P group σ_l data.

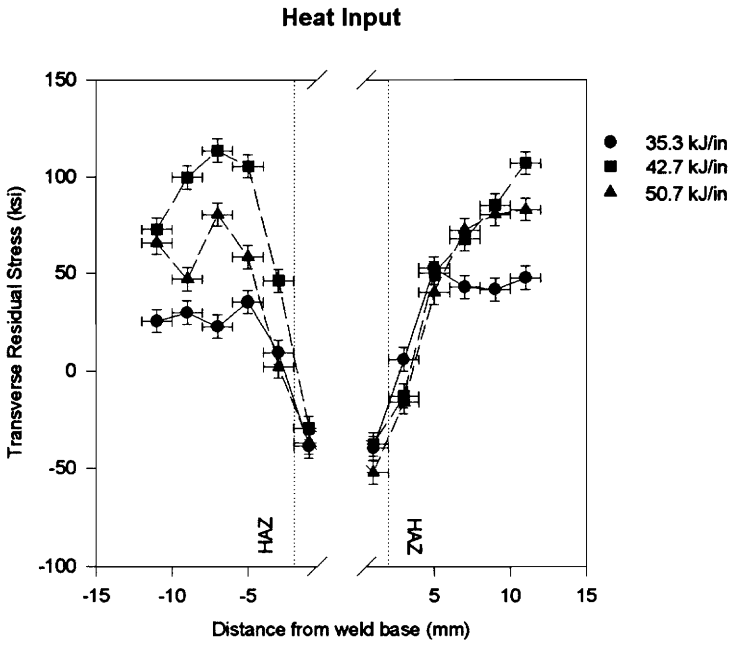

Figure 32. RS-H group σ_t data.

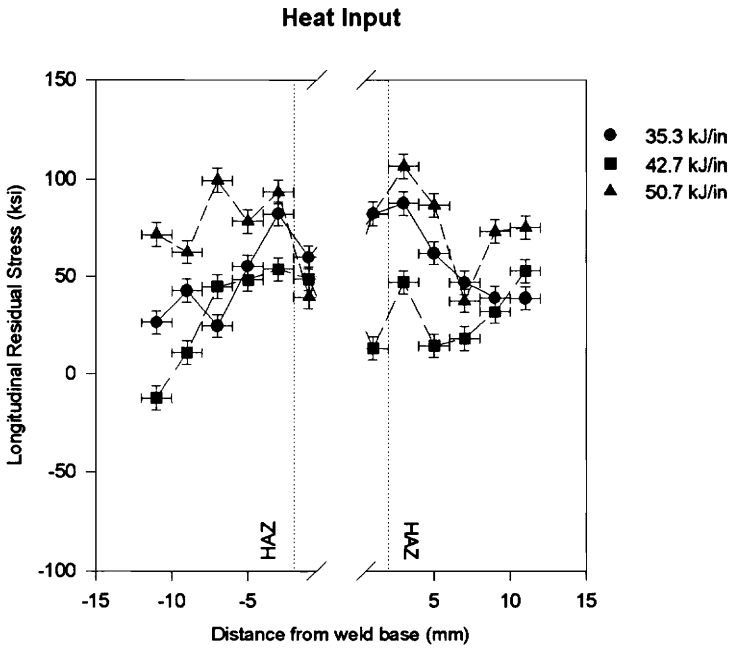

Figure 33. RS-H group σ_l data.

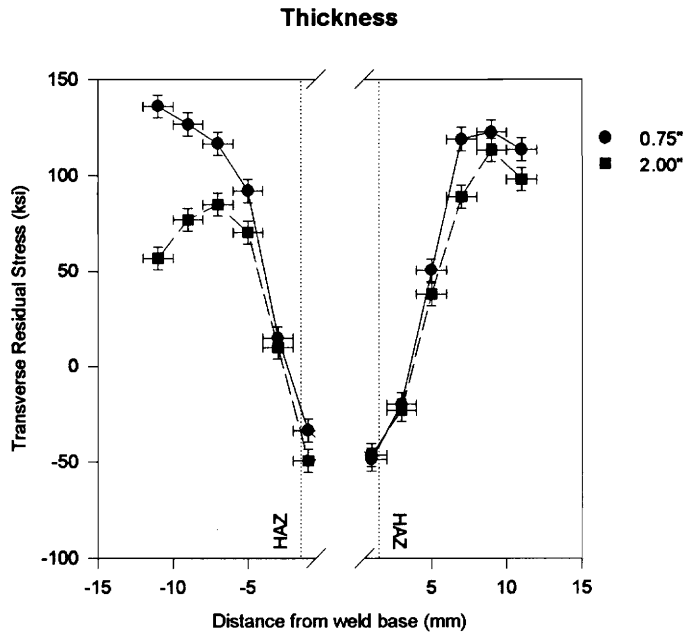

Figure 34. RS-T group σ_t data.

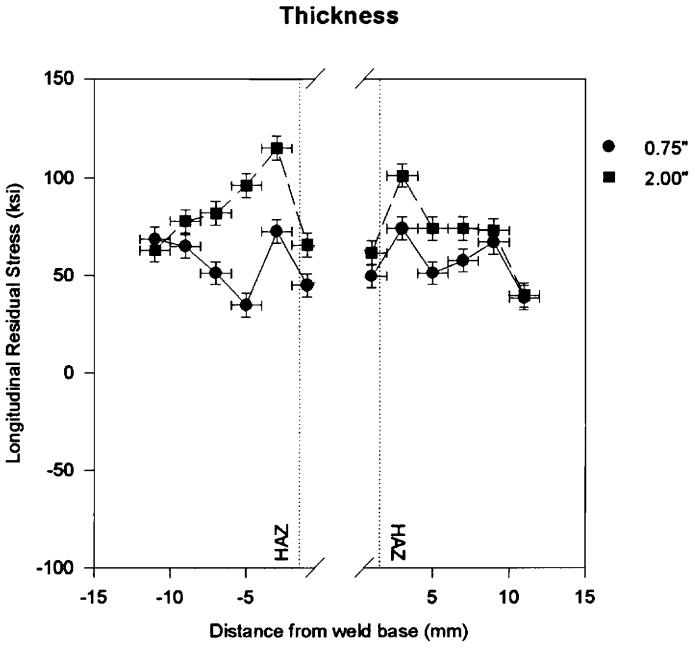

Figure 35. RS-T group σ_l data.

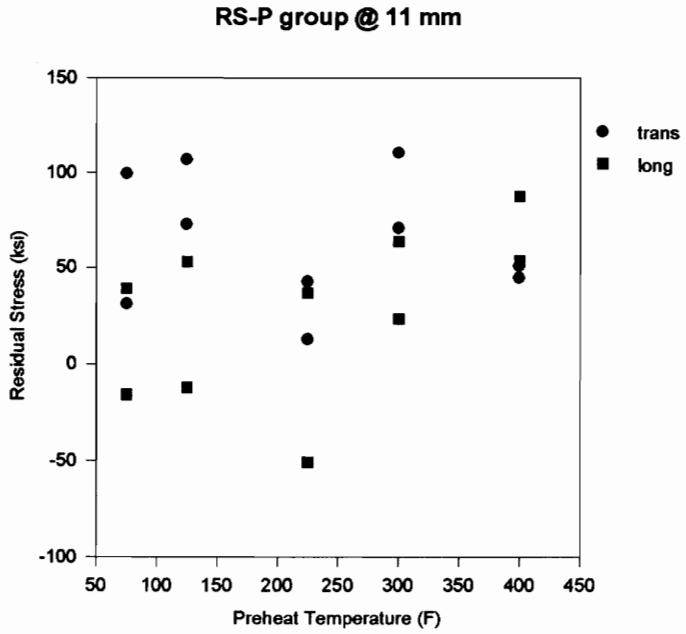

Figure 36. Residual stress data at 11 mm from weld base plotted versus preheat temperature.

6. CONCLUSIONS

Welding process parameters such as heat input and preheat temperature effect the surface residual state generated. However, pre-grinding a surface to be welded induces large surface and sub-surface residual stresses. The heat associated with welding interacts with the grinding residual stresses to create a final residual stress state very different than that which would be created exclusively by the welding process. Of all of the processing parameters, grinding has the largest effect of the residual stress state generated. This is unfortunate because the grinding is the least controlled aspect of the welding process. Grinding angle and force are purely at the discretion of the operator, and any variation in the grinding will be apparent in the residual stresses induced.

Much work has gone into the study of residual stresses induced by the welding process. In most instances, grinding was not performed or the stresses were relieved by annealing before welding residual stresses were determined. This is perfectly acceptable for the scientific study of residual stresses caused by the welding process. However, in actual shipbuilding or other welding applications where pre-grinding a surface to be welded is standard operating procedure, the final residual stress state will be very unlike what would be expected due to welding only. As was shown here, the differences between residual stresses due to welding and those due to grinding and welding can be very severe, and possibly detrimental to the structural stability of the welded construction. In most instances, the resulting residual stresses were highly tensile in nature, sometimes including large stress gradients near the weld bead.

The residual stress state of an unwelded sample of HSLA-100 base material was determined to be -15.2 ksi. The magnitude of these stresses did not change with annealing at 1200°F. For bead-on-plate weldments, assuming that the stresses closest to the weld bead are exclusively residual stresses due to welding, preheat temperature reduced the tensile nature, or increased the compressive nature, of the residual stresses. This is due to the preheat reducing the effect of shrinkage stresses induced after the austenite transformation upon cooling of the weldment. Be-

cause of the effects of grinding and the small sample sizes, no definitive conclusions could be drawn about the effects of heat input and plate thickness. It was shown that grinding was the dominant parameter on the residual stress state in these HSLA-100 bead-on-plate weldments. Because the angle and force of grinding are purely at the discretion of the operator, it is very difficult to determine the effects of different welding parameters on the residual stresses generated in bead-on-plate weldments ground prior to welding.

7. RECOMMENDATIONS

The knowledge gained throughout these experiments may be used to help guide future work. It was determined that the dominating factor in the generation of residual stresses in weldments was the severe, non-uniform grinding performed on the base metal in order to prepare a surface for welding. Because this is standard operating procedure, this grinding must be somehow controlled if the relationship between residual stresses and welding in actual engineering applications is to be determined. If only the relationship between welding parameters and residual stress is important, grinding should not be performed or the grinding stresses should be relieved in preparation for welding. However, if it is a goal to understand the causes and effects of welding residual stresses in actual shipbuilding applications, either the grinding process must be standardized and/or the complex interaction between residual stresses due to welding and those due to grinding must be investigated further.

When studying the effects of different processing parameters on the residual stress state generated in HSLA-100 bead-on-plate weldments, the number of levels for each welding parameter to be studied should be increased to at least four, thus heightening the certainty of the resulting conclusions and increasing the knowledge gained. In the case of studying heat input, the range of different heat inputs should be increased in order to better gain a comprehensive knowledge of how this effects residual stress.

8. APPENDIX A: TABULATED RAW DATA

Table 8. SR-1 post-weld residual stress data.

SR-1	σ_t (ksi)		σ_l (ksi)	
Distance	Line 1	Line 2	Line 1	Line 2
1 mm	-71.8	-69.3	-40.1	-26.8
	-73.0	-73.4	-37.9	-16.0
3 mm	-59.1	-47.6	-20.2	19.7
5 mm	-54.8	-49.6	-29.8	-30.9
	-61.7	-55.3	-42.4	-29.1
7 mm	-54.2	-54.5	-44.9	-43.4
9 mm	-55.5	-56.1	-47.4	-47.0
11 mm	-58.0	-49.2	-50..0	-45.0
	-53.9	-65.7	-59.3	-47.3

Table 9. SR-2 post-weld residual stress data.

SR-2	σ_t(ksi)					
Distance	Line 1	Line 2	Line 3	Line 4	Line 5	Line 6
1 mm	-10.2 -9.4	-20.2	-32.5	-18 -26	-21.1	-26.2
3 mm	7.7	-4.3	-12.2	-3.1	0.3	-4.6
5 mm	1.8 -15.7	-0.6	-7.8	-7.1 3.4	4.5	-3.4
7 mm	-5.8	-7.3	-10.1	1.8	6.4	-4.9
9 mm	-6.2	-6.8	-12.8	-1.2	7.5	-6.9
11 mm	-11.5 -17.8	-11.2	-15.5	-22.3 -9.6	-8.1	-12.6
SR-2	σ_l (ksi)					
Distance	Line 1	Line 2	Line 3	Line 4	Line 5	Line 6
1 mm	47.2 53.2	48.9	34.0	56.9 56.0	68.6	51.6
3 mm	26.0	59.0	54.7	58.3	65.0	25.3
5 mm	-6.3 -11.4	12.0	6.4	-6.1 -3.1	4.3 6.7	-27.0
7 mm	-31.7	-26.0	-29.5	-21.0	-28.6	-41.4
9 mm	-43.8	-42.2	-37.7	-44.6	-31.0	-54.5
11 mm	-47.5 -49.9	-49.1	-47.4	-53.6 -51.7		-53.3
12.5 mm					-61.6	

Table 10. RS-P1 residual stress data.

RS-P1	σ_t (ksi)		σ_l (ksi)	
Distance	Line 1	Line 2	Line 1	Line 2
1 mm	-19.0	-32.4	43.3	56.8
3 mm	14.0	-5.4	29.5	67.0
5 mm	41.2	55.2	-3.2	48.9
7 mm	33.7	96.3	-8.4	27.0
9 mm	24.5	82.1	-11.3	11.8
11 mm	31.2	99.5	-16.1	39.1

Table 11. RS-P2 residual stress data.

RS-P2	σ_t (ksi)		σ_l (ksi)	
Distance	Line 1	Line 2	Line 1	Line 2
1 mm	-37.5	-29.1	13.1	48.9
3 mm	-12.7	46.2	47.2	53.9
5 mm	50.1	105.6	14.4	48.4
7 mm	67.6	113.8	18.1	45.0
9 mm	85.5	99.8	32.0	11.0
11 mm	107.1	72.9	52.9	-12.4

Table 12. RS-P2 σ_t data.

RS-P2	σ_t (ksi)					
Distance	Line 1	Line 2	Line 3	Line 4	Line 5	Line 6
1 mm	-41.5	-41.7	-24.0	-27.7	-25.2	-28.2
	-43.9	-37.3	-27.4	-37.4		
	-32.9	-49.6	-31.2	-38.1		
	-17.3	-37.7		-30.6		
	-26.2	-32.8		-33.5		
	-24.3			-32.2		
	-39.0			-30.9		
	-37.5			-32.4		
				-39.9		
				-39.7		
				-34.0		
				-29.1		
3 mm	47.5	39.3	56.5	45.6	48.7	53.8
	6.8	36.1		46.2		
	-12.7					
5 mm	70.4	107.4	108.7	104.0	81.2	95.6
	50.1	116.3		105.6		
7 mm	96.3	119.9	119.9	123.9	88.7	97.9
	67.6	85.3		113.8		
9 mm	119.4	131.2	131.8	114.2	82.7	83.8
	113.9	72.9		99.8	82.0	80.8
	85.5					
11 mm	129.4	137.1	119.6	77.7	14.4	7.1
	127.7	126.2	112.1	80.9		
	123.4	120.2	111.3	72.9		
	133.6	101.1	86.4			
	109.1					
	104.3					
	107.6					
	107.1					

Table 13. RS-P2 σ_1 data.

RS-P2	σ_1 (ksi)					
Distance	Line 1	Line 2	Line 3	Line 4	Line 5	Line 6
1	55.3	73.3	49.5	40.9	54.2	45.7
	46.9	63.0	52.7	48.9		
	53.6	38.6	38.6			
	37.5					
	32.9					
	30.9					
	13.1					
3	51.3	59.1	50.2	61.3	64.9	45.2
	69.2			53.9		
	47.2					
5	38.3	54.0	47.9	43.4	31.8	39.5
	56.2			48.4		
	20.3					
	14.4					
7	43.4	21.3	47.7	38.5	27.4	20.6
	18.1			45.0		
9	64.3	22.6	29.2	41.7	27.5	6.2
	32.0			11.0		
11	43.4	55.2	24.5	11.4		
	55.5	57.9	12.1	-12.4		
	52.6	53.8	-3.8			
	47.3					
	52.9					

Table 14. RS-P3 residual stress data.

RS-P3	σ_t (ksi)		σ_l (ksi)	
Distance	Line 1	Line 2	Line 1	Line 2
1 mm	-54.7	-44.2	29.6	34.1
3 mm	-27.2	-25.4	66.8	59.2
5 mm	47.7	20.5	30.1	71.4
7 mm	89.4	46.7	49.8	10.7
9 mm	95.9	28.2	34.8	-50.8
11 mm	42.6	12.7	-51.0	36.8

Table 15. RS-P4 residual stress data.

RS-P4	σ_t (ksi)		σ_l (ksi)	
Distance	Line 1	Line 2	Line 1	Line 2
1 mm	-47.1	-34.7	30.9	23.7
3 mm	6.8	-39.1	86.7	95.5
5 mm	90.4	7.1	83.3	53.9
7 mm	109.1	66.0	82.3	41.2
9 mm	95.2	99.7	43.6	52.5
11 mm	71.0	110.6	23.4	63.9

Table 16. RS-P5 residual stress data.

RS-P5	σ_t (ksi)		σ_l (ksi)	
Distance	Line 1	Line 2	Line 1	Line 2
1 mm	-64.3	-35.2	-3.6	55.9
3 mm	-38.1	-41.7	81.4	105.0
5 mm	9.6	-4.6	78.6	92.0
7 mm	44.5	30.8	72.3	83.4
9 mm	58.1	47.2	54.7	78.1
11 mm	44.7	50.5	53.7	87.6

Table 17. RS-T1 residual stress data.

RS-T1	σ_t (ksi)		σ_l (ksi)	
Distance	Line 1	Line 2	Line 1	Line 2
1 mm	-48.7	-33.8	49.6	44.9
3 mm	-19.9	15.0	74.2	72.6
5 mm	50.6	92.2	51.2	34.9
7 mm	119.0	116.9	57.7	51.2
9 mm	122.7	126.7	67.2	65.0
11 mm	113.8	136.1	38.5	68.7

Table 18. RS-T2 residual stress data.

RS-T2	σ_t (ksi)		σ_l (ksi)	
Distance	Line 1	Line 2	Line 1	Line 2
1 mm	-49.5	-46.5	65.8	61.8
3 mm	9.9	-23.2	115.2	101.1
5 mm	70.5	37.9	96.1	74.1
7 mm	85.1	89.1	82.0	74.1
9 mm	77.2	113.5	77.8	73.1
11 mm	56.9	98.1	63.0	39.8

Table 19. RS-H1 residual stress data.

RS-H1	σ_t (ksi)		σ_l (ksi)	
Distance	Line 1	Line 2	Line 1	Line 2
1 mm	-39.5	-38.5	82.3	60.1
3 mm	6.0	9.6	87.7	82.3
5 mm	52.7	35.3	62.2	55.4
7 mm	42.9	22.7	47.0	24.5
9 mm	41.6	29.9	39.1	42.9
11 mm	47.6	25.5	38.9	26.4

Table 20. RS-H2 residual stress data.

RS-H2	σ_t (ksi)		σ_l (ksi)	
Distance	Line 1	Line 2	Line 1	Line 2
1 mm	-51.9	-36.6	82.4	39.7
3 mm	-15.8	2.2	106.3	93.6
5 mm	40.2	58.5	86.7	78.5
7 mm	72.5	80.6	37.6	99.4
9 mm	80.6	47.0	73.4	62.8
11 mm	83.2	65.8	75.3	71.8

REFERENCES

[1] Czyryca, E.J., R.E. Line, and R.J. Wong, "Evaluation of HSLA-100 Steel for Surface Combatant Structural Certification," David Taylor Research Center Report, DTRC/SME-89/15, Bethesda, Maryland, p. 3, (1989).

[2] Blackburn, J., "Weld Residual Stresses, Measurement, Characterization, and Prediction," Presentation at National Institute of Standards and Technology, March 29, 1993.

[3] Poole, S.W. and J.E. Franklin, "High-Strength Structural and High-Strength Low-Alloy Steels," *Metals Handbook, vol. 1*, ASM, Metals Park, pp. 403-420, (1978).

[4] Smith, W.F., *Structure and Properties of Engineering Alloys, 2nd ed.*, McGraw-Hill, New York, p. 114, (1993).

[5] Czyryca, E.J., et. al., p. 4.

[6] Fletcher, E.E., *High-Strength, Low-Alloy Steels: Status, Selection and Physical Metallurgy*, Battelle Press, Columbus, p. 6, (1979).

[7] Reynolds, W.T., personnel communication, (1993).

[8] Smith, W.F., p. 114.

[9] Fletcher, E.E., p. 2.

[10] Mordfin, L., "Measurement of Residual Stresses: Problems and Opportunities," *Residual Stress for Designers and Metallurgists*, L.J. VandeWalle, ed., ASM, Metals Park, pp. 189-209, (1981).

[11] Winholtz, R.A. and J.B. Cohen, "Load Sharing of the Phases in 1080 Steel during Low-Cycle Fatigue," *Metallurgical Transactions A*, vol. 23A, pp. 341-354, (January 1992).

[12] Mordfin, L., pp. 189-209.

[13] Leggatt, R.H., "Residual Stress and Distortion in Multipass Butt Welded Joints in Type 316 Stainless Steel," *Residual Stresses in Science and Technology*, Garmisch-Partenkirchen, Oberursel, Germany, E. Macherauch and V. Hauk eds., pp. 997-1004, (1987).

[14] Brand, P.C., Th.H. De Keijser, and G. Den Ouden, "Residual Stresses and Plastic Deformation in GTA-Welded Steel," *Welding Journal, Welding Research Supplement*, pp. 93-s–100-s, (March 1993).

[15] Crostack, H.-A. and W. Reimers, "Residual Stress Profile from Grain to Grain in a Welding Zone," Proceedings of the Second International Conference on Residual Stress, *ICRS2*, November 1988, Nancy, France, G. Beck, S. Denis and A. Simon eds., Elsevier Applied Science Publishing Company, pp. 58-64, (1989).

[16] Nitschke, Th., and H. Wohlfahrt, "Residual Stress Distributions After Welding as a Consequence of the Combined Effect of Physical Metallurgical and Mechanical Sources," *Mechanical Effects of Welding*, IUTAM Symposium, Lulea/Sweden, 1991, L. Karlsson, L.-E. Lindgren, M. Jonsson, eds., Springer-Verlag, Berlin, pp. 123-134, (1992).

[17] Heeschen, J., T. Nitschke, and H. Wohlfahrt, "New Results on the Formation of Residual Stresses due to Phase Transformations in the Welded Structural Steels St 52-3 and StE 690," *Residual Stresses in Science and Technology*, Garmisch-Partenkirchen, Oberursel, Germany, E. Macherauch and V. Hauk eds., pp. 1005-1013, (1987).

[18] Nitschke, Th., et. al., pp. 123-134.

[19] Masubuchi, K., *Analysis of Welded Structures, Residual Stresses, Distortion, and their Consequences*, Pergamon Press, Oxford, p. 80, (1980).

[20] Brand, P.C., et. al., pp. 93-s–100-s.

[21] Heeschen, J., et. al., pp. 1005-1013.

[22] Masubuchi, K., p. 532.

[23] Brand, P.C., et. al., pp. 93-s–100-s.

[24] Blackburn, J., personal communication, (1994).

[25] Dahl, W. and H. Krebs, "Determination and Assessment of Residual Stresses in a Multilayer Submerged Arc Welded Joint," Proceedings of the Second International Conference on Residual Stress, *ICRS2*, November 1988, Nancy, France, G. Beck, S. Denis and A. Simon eds., Elsevier Applied Science Publishing Company, pp. 683-689, (1989).

[26] Wohlfahrt, H., "Residual Stresses due to Welding: their Origin, Calculation and Evaluation," Papers presented at the European Conference on Residual Stress, *Residual Stresses*, 1983, Karlsruhe, Germany, E. Macherauch and V. Hauk eds., DGM Informationsgesellschaft, pp. 81-112, (1986).

[27] Hendricks, R.W., J. Jo, V.S. Iyer, and D.P. Vijay, "Residual Stresses in Austenitic Stainless Steels: A Review of Experimental Techniques," Report RSL-90-006, prepared for Martin Marietta Energy Systems, Oak Ridge, TN, (1991).

[28] Ruud, C.O. and G.D. Farmer, "Residual Stress Measurement by X-Rays: Errors, Limitations and Applications," *Nondestructive Evaluation of Materials*, J.J. Burke and V. Weiss eds., Plenum Press, N.Y., (1979).

[29] Cohen, J.B., "X-ray Techniques for the Measurement of Residual Stresses in the Real World," *Residual Stress for Designers and Metallurgists*, L.J. VandeWalle ed., ASM, Metals Park, pp. 211-221, (1981).

[30] Cohen, J.B., pp. 211-221.

[31] Jo, J., and R.W. Hendricks, "Diffractometer Misalignment Errors in X-ray Residual Stress Measurements," *Journal of Applied Crystallography*, vol. 24, pp. 878-887, (1991).

[32] Noyan, I.C., and J.B. Cohen, *Residual Stress, Measurement by Diffraction and Interpretation*, Springer-Verlag, New York, p. 121., (1987).

[33] Noyan, I.C., et. al., p.122.

[34] Czyryca, E.J. et. al., pp. 133-134.

[35] Czyryca, E.J. et. al., pp. 3-5.

[36] Czyryca, E.J. et. al., pp. 110-112.

[37] Czyryca, E.J. et. al., p. 46.

[38] Czyryca, E.J. et. al., p. 47.

[39] Noyan, I.C., et. al., p. 110.

[40] Czyryca, E.J. et. al., pp. 44-47.

[41] Czyryca, E.J. et. al., p. 63.

[42] James, M. And J.B. Cohen, "PARS-A Portable X-ray Analyzer for Residual Stresses," *Journal of Testing and Evaluation*, JTEVA, vol. 6, no. 2, pp. 91-97, (March 1978).

[43] *TEC Model 1600 X-ray Stress Analysis System Operation and Maintenance Manual*, Technology for Energy Corp., Knowxville, TN, p. C-6, (1985).

[44] Blackburn, J., personnel communication (1993).

[45] Noyan, I.C., et. al., pp. 164.

[46] Noyan, I.C., et. al., pp. 181.

[47] Kuznetsov, E.N., "Residual Stresses in Long Weldments," *Residual Stress for Designers and Metallurgists*, L.J. VandeWalle, ed., ASM, Metals Park, pp. 91-104, (1981).

[48] Yoshihisa, E., "Residual Stress Measurements of Welded Plates by X-ray and Hole Drilling Techniques," Proceedings of the Third International Conference on Residual Stress, *ICRS3*, July 1991, Tokushima, Japan, H. Fujiwara, T. Abe and K. Tanaka, eds., Elsevier Applied Science Publishing Company, pp. 979-984, (1992).

[49] Varughese, R., and P.R. Howell, "The Application of Transmission Electron Microscopy to the Study of a Low Carbon Steel: HSLA-100," to be published in: *Metallography: 75 Years Later*, ASTM, Philadelphia.

[50] Walker, E.D. "Some Aspects of Residual Stress in Parts Heat Treated by the Induction Method," *Residual Stress for Designers and Metallurgists*, Metals Park: American Society for Metals, p. 41-50, (1981).

[51] Scholtes, Berthold. "Residual Stresses Introduced by Machining," *Advances in Surface Treatments, vol. 4, Residual Stresses*, France: Pergamon Press, p. 59-72, c. 1987.

[52] Masubuchi, K., p. 93.

[53] Courtney, S., "An In-line, Non-destructive Procedure to Detect Camshaft Lobe Grinding Burn," MSc Thesis, Materials Science and Engineering Department, Virginia Polytechnic Institute and State University, Blacksburg, Virginia (May, 1993).

[54] Chrenko, R.M., "Residual Stress Studies of Austenitic and Ferritic Steels," Residual Stresses in Welded Construction and Their Effects, International conference, London, November 15-17, 1977, The Welding Institute, Abington Hall, pp. 79-88, (1978).

[55] Wohlfahrt, H., pp. 81-112.

[56] Wohlfahrt, H., pp. 81-112.

[57] Brand, P.C., et. al., pp. 93-S−100-s.

[58] Nitschke, Th., et. al., pp. 123-134.

VITA

The author was born May 29, 1969 in Fairfax, Virginia to Sandra L. and David R. Cunningham. He lived in the eastern end of the formerly rural Loudoun County, Virginia from the time he was two years of age, until graduating from Broad Run High School in Ashburn in 1987. Upon completing his grade-school education, the author chose to come to Blacksburg to pursue a degree in engineering from Virginia Polytechnic Institute and State University. A bachelor's of science in Materials Engineering was received in May of 1991. Not satisfied with the knowledge gained, he enrolled in the graduate school to pursue a master's degree in Material Science and Engineering. Upon completion of this work, the author will move to Lake Park, Florida, gain employment, and marry his fiancée.